12 Liew CG, Shah NN, Briston SJ et al. PAX4 enhances β-cell differentiation of human embryonic stem cells. PLoS ONE 2008;3:e1783.
13 Chung S, Sonntag KC, Andersson T et al. Genetic engineering of mouse embryonic stem cells by Nurr1 enhances differentiation and maturation into dopaminergic neurons. Eur J Neurosci 2002;16: 1829–1838.
14 Kovesdi I, Brough DE, Bruder JT et al. Adenoviral vectors for gene transfer. Curr Opin Biotechnol 1997;8:583–589.
15 Benihoud K, Yeh P, Perricaudet M. Adenovirus vectors for gene delivery. Curr Opin Biotechnol 1999;10:440–447.
16 Kawabata K, Sakurai F, Yamaguchi T et al. Efficient gene transfer into mouse embryonic stem cells with adenovirus vectors. Mol Ther 2005;12:547–554.
17 Tashiro K, Kawabata K, Sakurai H et al. Efficient adenovirus vector-mediated PPAR gamma gene transfer into mouse embryoid bodies promotes adipocyte differentiation. J Gene Med 2008;10:498–507.
18 Tontonoz P, Hu E, Spiegelman BM. Stimulation of adipogenesis in fibroblasts by PPAR γ2, a lipid-activated transcription factor. Cell 1994;79:1147–1156.
19 Rosen ED, Sarraf P, Troy AE et al. PPARγ is required for the differentiation of adipose tissue in vivo and in vitro. Mol Cell 1999;4: 611–617.
20 Mizuguchi H, Kay MA. Efficient construction of a recombinant adenovirus vector by an improved in vitro ligation method. Hum Gene Ther 1998;9:2577–2583.
21 Mizuguchi H, Kay MA. A simple method for constructing E1- and E1/E4-deleted recombinant adenoviral vectors. Hum Gene Ther 1999; 10:2013–2017.
22 Niwa H, Yamamura K, Miyazaki J. Efficient selection for high-expression transfectants with a novel eukaryotic vector. Gene 1991; 108:193–199.
23 Sakurai H, Tashiro K, Kawabata K et al. Adenoviral expression of suppressor of cytokine signaling-1 reduces adenovirus vector-induced innate immune responses. J Immunol 2008;180:4934–4938.
24 Tashiro K, Kondo A, Kawabata K et al. Efficient osteoblast differentiation from mouse bone marrow stromal cells with polylysin-modified adenovirus vectors. Biochem Biophys Res Commun 2009;379: 127–132.
25 Maizel JV Jr, White DO, Scharff MD. The polypeptides of adenovirus. I. Evidence for multiple protein components in the virion and a comparison of types 2, 7A, and 12. Virology 1968;36:115–125.
26 Aoi T, Yae K, Nakagawa M et al. Generation of pluripotent stem cells from adult mouse liver and stomach cells. Science 2008;321:699–702.
27 Dani C, Smith AG, Dessolin S et al. Differentiation of embryonic stem cells into adipocytes in vitro. J Cell Sci 1997;110(Pt 11): 1279–1285.
28 Kawaguchi J, Mee PJ, Smith AG. Osteogenic and chondrogenic differentiation of embryonic stem cells in response to specific growth factors. Bone 2005;36:758–769.
29 Bergelson JM, Cunningham JA, Droguett G et al. Isolation of a common receptor for Coxsackie B viruses and adenoviruses 2 and 5. Science 1997;275:1320–1323.
30 Tomko RP, Xu R, Philipson L. HCAR and MCAR: the human and mouse cellular receptors for subgroup C adenoviruses and group B coxsackieviruses. Proc Natl Acad Sci USA 1997;94:3352–3356.
31 Mizuguchi H, Hayakawa T. Targeted adenovirus vectors. Hum Gene Ther 2004;15:1034–1044.
32 Ducy P, Zhang R, Geoffroy V et al. Osf2/Cbfa1: a transcriptional activator of osteoblast differentiation. Cell 1997;89:747–754.
33 Komori T, Yagi H, Nomura S et al. Targeted disruption of Cbfa1 results in a complete lack of bone formation owing to maturational arrest of osteoblasts. Cell 1997;89:755–764.
34 zur Nieden NI, Kempka G, Ahr HJ. In vitro differentiation of embryonic stem cells into mineralized osteoblasts. Differentiation 2003;71: 18–27.
35 Chung S, Andersson T, Sonntag KC et al. Analysis of different promoter systems for efficient transgene expression in mouse embryonic stem cell lines. Stem Cells 2002;20:139–145.
36 Rust EM, Westfall MV, Samuelson LC et al. Gene transfer into mouse embryonic stem cell-derived cardiac myocytes mediated by recombinant adenovirus. In Vitro Cell Dev Biol Anim 1997;33:270–276.
37 Hong S, Hwang DY, Yoon S et al. Functional analysis of various promoters in lentiviral vectors at different stages of in vitro differentiation of mouse embryonic stem cells. Mol Ther 2007;15: 1630–1639.
38 Brooks AR, Harkins RN, Wang P et al. Transcriptional silencing is associated with extensive methylation of the CMV promoter following adenoviral gene delivery to muscle. J Gene Med 2004;6: 395–404.
39 Rufaihah AJ, Haider HK, Heng BC et al. Directing endothelial differentiation of human embryonic stem cells via transduction with an adenoviral vector expressing the VEGF(165) gene. J Gene Med 2007; 9:452–461.
40 Brokhman I, Pomp O, Shaham L et al. Genetic modification of human embryonic stem cells with adenoviral vectors: differences of infectability between lines and correlation of infectability with expression of the coxsackie and adenovirus receptor. Stem Cells Dev 2009;18: 447–456.
41 Tai G, Polak JM, Bishop AE et al. Differentiation of osteoblasts from murine embryonic stem cells by overexpression of the transcriptional factor osterix. Tissue Eng 2004;10:1456–1466.
42 Nakashima K, Zhou X, Kunkel G et al. The novel zinc finger-containing transcription factor osterix is required for osteoblast differentiation and bone formation. Cell 2002;108:17–29.
43 Marie PJ. Transcription factors controlling osteoblastogenesis. Arch Biochem Biophys 2008;473:98–105.
44 Mauritz C, Schwanke K, Reppel M et al. Generation of functional murine cardiac myocytes from induced pluripotent stem cells. Circulation 2008;118:507–517.
45 Narazaki G, Uosaki H, Teranishi M et al. Directed and systematic differentiation of cardiovascular cells from mouse induced pluripotent stem cells. Circulation 2008;118:498–506.
46 Schenke-Layland K, Rhodes KE, Angelis E et al. Reprogrammed mouse fibroblasts differentiate into cells of the cardiovascular and hematopoietic lineages. Stem Cells 2008;26:1537–1546.
47 Stadtfeld M, Nagaya M, Utikal J et al. Induced pluripotent stem cells generated without viral integration. Science 2008;322:945–949.
48 Okita K, Nakagawa M, Hyenjong H et al. Generation of mouse induced pluripotent stem cells without viral vectors. Science 2008; 322:949–953.

See www.StemCells.com for supporting information available online.

Biochemical and Biophysical Research Communications 379 (2009) 127–132

Contents lists available at ScienceDirect

Biochemical and Biophysical Research Communications

journal homepage: www.elsevier.com/locate/ybbrc

Efficient osteoblast differentiation from mouse bone marrow stromal cells with polylysin-modified adenovirus vectors

Katsuhisa Tashiro [a,b], Asami Kondo [a], Kenji Kawabata [a], Haruna Sakurai [a,b], Fuminori Sakurai [a], Koichi Yamanishi [b,c], Takao Hayakawa [d,e], Hiroyuki Mizuguchi [a,b,*]

[a] Laboratory of Gene Transfer and Regulation, National Institute of Biomedical Innovation, 7-6-8 Saito-Asagi, Ibaraki, Osaka 567-0085, Japan
[b] Graduate School of Pharmaceutical Sciences, Osaka University, 1-6 Yamadaoka, Suita, Osaka 565-0871, Japan
[c] National Institute of Biomedical Innovation, 7-6-8 Saito-Asagi, Ibaraki, Osaka 567-0085, Japan
[d] Pharmaceutics and Medical Devices Agency, 3-3-2, Kasumigaseki, Chiyoda-Ku, Tokyo 100-0013, Japan
[e] Pharmaceutical Research and Technology Institute, Kinki University, 3-4-1. Kowakae, Higashi-Osaka, Osaka 577-8502, Japan

ARTICLE INFO

Article history:
Received 2 December 2008
Available online 25 December 2008

Keywords:
Fiber-modified adenovirus vectors
Bone marrow stromal cells
Osteoblasts

ABSTRACT

Bone marrow stromal cells (BMSCs) are expected to be a source for tissue regeneration because they can differentiate into multiple cell types. Establishment of efficient gene transfer systems for BMSCs is essential for their application to regenerative medicine. In this study, we compared the transduction efficiency in mouse primary BMSCs by using fiber-modified adenovirus (Ad) vectors, and demonstrated that AdK7, which harbors a polylysin (K7) peptide in the C-terminus of the fiber knob, could efficiently express a transgene in BMSCs. Notably, AdK7 robustly drove transgene expression in more than 90% of the BMSCs at 3,000 vector particles/cell. Furthermore, we showed that *in vitro* and *in vivo* osteogenic potential of BMSCs was dramatically promoted by the transduction of Runx2 gene using AdK7. These results indicate that this transduction system could be a powerful tool for therapeutic applications based on BMSCs.

Because bone marrow stromal cells (BMSCs) containing mesenchymal stem cells (MSCs) can be easily isolated from adult tissues and efficiently expanded *in vitro*, and can differentiate into multiple cell types [1,2], BMSCs are expected to be an ideal source of cells for the regeneration of tissues. However, it is difficult to obtain a large amount of pure differentiated cells from BMSCs because of their low differentiation efficiency. The cell transition from stem cells to lineage-committed cells involves many transcription factors that promote or suppress cellular differentiation [3]. Thus, to develop an efficient method for differentiating from BMSCs into specialized cells, we planned to combine the transduction of a functional gene, which promotes cellular differentiation, with stimulation by chemical reagents. To do this procedure, it is essential to develop efficient transduction systems for BMSCs.

Among the various types of gene delivery vectors, adenovirus (Ad) vectors have been widely used for gene transfer studies, since they can achieve high transduction efficiency and transduce both dividing and non-dividing cells [4]. Although Ad vector-mediated transduction into BMSCs has been performed, the transduction efficiency was found to be lower than those of many other cell lines [5,6]. This is due to the low levels of coxsackievirus and adenovirus receptor (CAR), which mediates adenovirus entry, on the cell surface [5,6]. To overcome this problem, we and others have generated several types of fiber-modified Ad vectors, which mediate efficient gene transduction into the cells expressing very low levels of CAR [7,8]. Transduction efficiency was improved in various types of the cells by the insertion of Arg-Gly-Asp (RGD) peptide or 7-tandem lysine residues (KKKKKKK: K7) peptide, which targets αv integrins or heparan sulfates, respectively, on the cell surface, into the fiber knob of the Ad vector [7,8]. In particular, we previously reported that polylysin-modified Ad vector (AdK7) is the most suitable vector for transduction into human bone marrow-derived MSCs (hMSCs) [9].

In this study, we initially investigated the transduction efficiency of mouse primary BMSCs by using fiber-modified Ad vectors. We next examined whether the osteogenic potential of BMSCs was promoted by using Ad vector-mediated transduction of a runt-related transcription factor 2 (Runx2) gene, which is known as a master gene for osteoblastogenesis [10,11].

Materials and methods

Ad vectors. Ad vectors were constructed using an improved *in vitro* ligation method [12,13]. The CA (cytomegalovirus (CMV) enhancer/β-actin promoter) promoter [14]-driven β-galactosidase

* Corresponding author. Address: Laboratory of Gene Transfer and Regulation, National Institute of Biomedical Innovation, 7-6-8 Saito-Asagi, Ibaraki, Osaka 567-0085, Japan. Fax: +81 72 641 9816.
E-mail address: mizuguch@nibio.go.jp (H. Mizuguchi).

0006-291X/$ - see front matter © 2008 Elsevier Inc. All rights reserved.
doi:10.1016/j.bbrc.2008.12.055

(LacZ)-expressing plasmid, pHMCA-LacZ [15], was digested with I-*Ceu*I/PI-*Sce*I and inserted into I-*Ceu*I/PI-*Sce*I-digested pAdHM15-RGD [16] or pAdHM41-K7 (C) [8], resulting in pAdRGD-CA-LacZ, pAdK7-CA-LacZ, respectively. The CMV or the human elongation factor (EF)-1α promoter-driven LacZ-expressing plasmid, pHMCMV-LacZ [15] or pHMEF-LacZ [15], respectively, was also digested with I-*Ceu*I/PI-*Sce*I and ligated into I-*Ceu*I/PI-*Sce*I-digested-pAdHM41-K7 (C), resulting in pAdK7-CMV-LacZ or pAdK7-EF-LacZ, respectively. The CA promoter-driven mouse Runx2-expressing plasmid, pHMCA-Runx2, was generated by inserting a mouse Runx2 cDNA, which is derived from pCMV-Runx2 (a kind gift from Dr. S. Takeda, Tokyo Medical and Dental University, Tokyo, Japan) [17], into pHMCA5. pHMCA-Runx2 was also digested with I-*Ceu*I/PI-*Sce*I, and inserted with pAdHM4 [12] or pAdHM41-K7 (C), resulting in pAd-CA-Runx2 or pAdK7-CA-Runx2, respectively. Ad vectors (Ad-CA-LacZ, AdRGD-CA-LacZ, AdK7-CA-LacZ, AdK7-CMV-LacZ, AdK7-EF-LacZ, Ad-CA-Runx2, and AdK7-CA-Runx2) were generated and purified as described previously [18]. Determination of virus particle (VP) and biological titer were determined using by a spectrophotometrical method [19] and by means of an Adeno-X Rapid Titer Kit (Clontech, Palo Alto, CA), respectively. The ratio of the biological-to-particle titer was 1:14 for Ad-CA-LacZ, 1:35 for AdRGD-CA-LacZ, 1:42 for AdK7-CA-LacZ, 1:25 for AdK7-CMV-LacZ, 1:32 for AdK7-EF-LacZ, 1:17 for Ad-CA-Runx2, and 1:28 for AdK7-CA-Runx2.

Mouse primary BMSCs. Primary BMSCs were harvested from female C57BL/6 mice (8 weeks; Nippon SLC, Shizuoka, Japan) as below. Femora and tibias were isolated and placed in Dulbecco's modified Eagle's medium (DMEM; Sigma, St. Louis, MO)/20% fetal bovine serum (FBS; Invitrogen, Carlsbad, CA) and 1% penicillin/streptomycin. Bone marrow was obtained by flushing these bones, and cells recovered from the bones of one animal were then seeded into a 150 mm tissue culture plate. Medium was changed every 2 days to remove non-adherent cells, and adherent cells were cultured until reaching confluence. At confluence, BMSCs were passaged after digestion with 0.25% trypsin/1 mM EDTA. BMSCs (passage 4–12) were subsequently used for further analysis.

LacZ assay. BMSCs (1×10^4 cells) were plated in 24-well plates. The next day, they were transduced with the indicated doses of Ad vectors for 1.5 hr. Two days later, X-gal staining and β-gal luminescence assays were performed as described previously [18].

Osteoblasts differentiation. BMSCs (1×10^4 cells) were plated in 24-well plates. Cells were transduced with 3000 VP/cell of Ad vector for 1.5 hr. After aspirating the viral solution, osteogenic differentiation medium, consisting of growth medium (DMEM/20% FBS) containing 50 μg/mL ascorbic acid 2-phosphate (Sigma), 5 mM β-glycerophosphate (Sigma), and 100 nM dexamethasone (Wako, Osaka, Japan), was added. The medium was replaced every 3 days.

von Kossa staining, calcium quantitation. Cells were fixed with 4% paraformaldehyde/phosphate-buffered saline (PBS) and stained with $AgNO_3$ by the von Kossa method. To measure calcium deposition, cells were washed twice with PBS and decalcified with 0.5 M acetic acid, and cell culture plates were rotated overnight at room temperature (R/T). Insoluble material was removed by centrifugation. The supernatants were then assayed for calcium with the calcium C-test Wako kit (Wako). DNA in pellets was extracted using the DNeasy tissue kit (Qiagen), and calcium content was then normalized to DNA.

ALP assay. Cells were lysed in 10 mM Tris–HCl (pH 7.5) containing 1 mM $MgCl_2$ and 0.1% Triton X-100, and the lysates were then used for assay. Alkaline phosphatase (ALP) activity was measured using the LabAssay ALP kit (Wako) according to the manufacturer's instructions. The protein concentration of the lysates was determined using a Bio-Rad assay kit (Bio-Rad laboratories, Hercules, CA), and ALP activity was then normalized by protein concentration.

RT-PCR. RT-PCR was performed as described previously [18]. The sequences of primers were as follows: Runx2(F), 5′-CCT CTG ACT TCT GCC TCT GG-3′; Runx2(R), 5′-CAG CGT CAA CAC CAT CAT TC-3′; osterix(F), 5′- CTT AAC CCA GCT CCC TAC CC-3′; osterix(R), 5′- TGT GAA TGG GCT TCT TCC TC-3′; bone sialoprotein(F), 5′- AAA GTG AAG GAA AGC GAC GA-3′; bone sialoprotein(R), 5′-GTT CCT TCT GCA CCT GCT TC-3′; osteocalcin(F), 5′-GCG CTC TGT CTC TCT GAC CT -3′; osteocalcin(R), 5′-TTT GTA GGC GGT CTT CAA GC-3′; collagen Iα1(F), 5′-CAC CCT CAA GAG CCT GAG TC-3′; collagen Iα1 (R), 5′-GCT ACG CTG TTC TTG CAG TG-3′, GAPDH(F), 5′-ACC ACA GTC CAT GCC ATC AC-3′; GAPDH(R), 5′-TCC ACC ACC CTG TTG CTG TA-3′.

Western blotting. Western blotting was performed as described previously [18]. Briefly, lysates (20 μg) were subjected to 12.5% polyacrylamide gel and were transferred to a polyvinylidene fluoride membrane (Millipore, Bedford, MA). After blocking with Immunoblock (DS Pharma Biomedical, Osaka, Japan) at R/T for 1 hr, the membrane was exposed to rabbit anti-Runx2 antibody (Santa Cruz Biotechnology, Inc., Santa Cruz, CA) at 4 °C overnight, followed by horseradish peroxidase-conjugated secondary antibody at R/T for 1 hr. The band was visualized by ECL Plus Western blotting detection reagents (Amersham Bioscience, Piscataway, NJ) and the signals were read using a LAS-3000 imaging system (FUJIFILM, Tokyo, Japan). All blots were stripped and reblotted with antibody against β-actin (Sigma) for normalization.

In vivo heterotopic bone formation. BMSCs (2×10^6 cells, passage 8–9) were transduced with AdK7-CA-LacZ, AdK7-CA-Runx2, or Ad-CA-Runx2, at 3000 VP/cells for 1.5 hr. The next day, cells were collected by trypsin, and resuspended in 150 μl of PBS, and then injected into the hind limb biceps muscle of nude mice (Nippon SLC) (2animal/ group). At 4–5 weeks after injection, mice were anesthetized by isofluorane and bone formation was analyzed with a microcomputed tomography (microCT) system (eXplore Locus CT System; GE Healthcare, London, ON, Canada). Both an X-ray image and a three-dimensional reconstitution image were obtained by using the microCT system.

Results

Optimization of transduction efficiency in BMSCs by using various types of Ad vectors

To optimize Ad vectors for transduction into BMSCs, we prepared three LacZ-expressing Ad vectors, Ad-CA-LacZ, AdRGD-CA-LacZ, and AdK7-CA-LacZ. We investigated the transduction efficiency of these Ad vectors in BMSCs at the indicated vector dose. X-gal staining showed that LacZ-positive cells were less than 10% even at a dose of 3000 vector particles (VP)/cell in Ad-CA-LacZ (Fig. 1A). On the other hand, more than 90% of the cells expressed LacZ at the same dose in AdK7-CA-LacZ. A luminescence assay revealed that, at 3000 VP/cell, the LacZ expression level in the cells transduced with AdRGD-CA-LacZ or AdK7-CA-LacZ was increased by about 5- or 50-fold, respectively, in comparison with that in the cells transduced with Ad-CA-LacZ (Fig. 1B). These results were quite similar to those of our previous report, in which efficient transduction in hMSCs was achieved by using AdK7 [9], and our data clearly demonstrated that AdK7 is a suitable vector for transduction into both mouse BMSCs and hMSCs.

We and others reported that the choice of promoters is important for transduction efficiency, especially in immature cells [15,18,20,21]. Thus, we examined the transduction efficiency by comparing the promoter activities in BMSCs. In addition to the CA promoter, we prepared LacZ-expressing AdK7 under the control of the CMV promoter or the EF-1α promoter (AdK7-CMV-LacZ or AdK7-EF-LacZ, respectively). A luminescent assay showed that the CA promoter represented the highest transgene expression

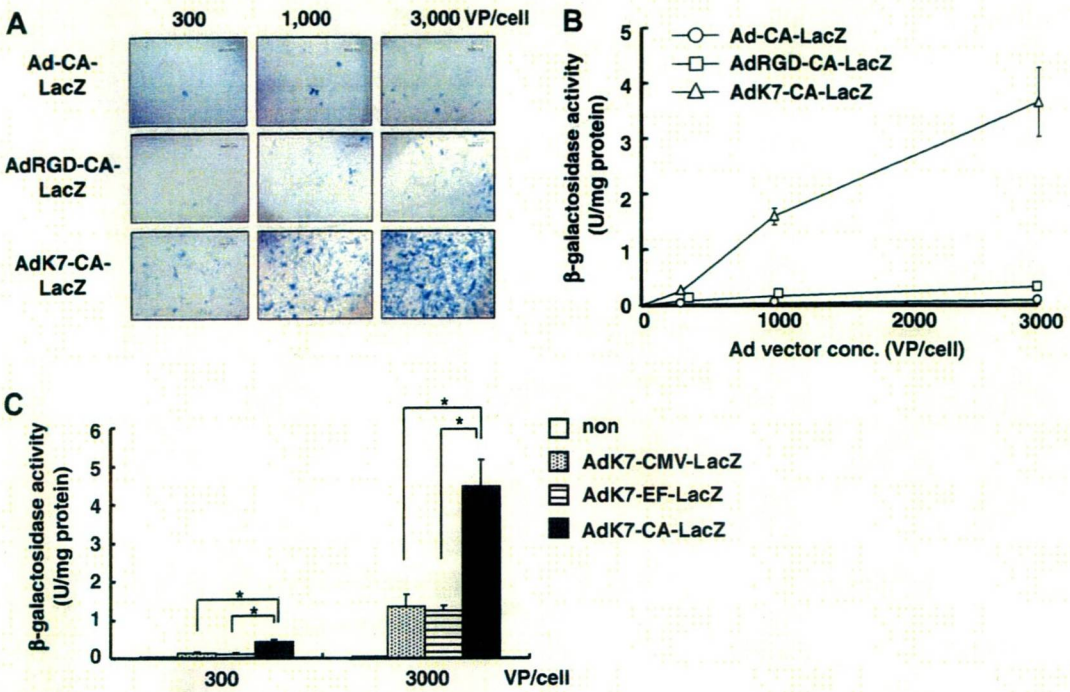

Fig. 1. Gene transduction efficiency in mouse primary BMSCs by various types of Ad vectors. Mouse BMSCs were transduced with the indicated doses of LacZ-expressing Ad vectors. Two days later, (A) X-gal staining and (B) luminescence assay were performed. Similar results of X-gal staining were obtained in three independent experiments. Scale bar indicates 200 μm. (C) Optimization of promoter activity in BMSCs using LacZ-expressing AdK7. BMSCs were transduced with the indicated dose of each Ad vector, and LacZ expression in the cells was measured. The data are expressed as mean ± S.D. ($n = 3$). $p < 0.01$.

among the three types of the promoters (Fig. 1C). These results demonstrate that AdK7 containing the CA promoter is the most effective at attaining high transduction efficiency in mouse BMSCs.

We also investigated the cytotoxicity in BMSCs transduced with AdK7-CA-LacZ. Almost no difference in cell number between non-transduced cells and AdK7-CA-LacZ-transduced cells was observed on day 2 after transduction (data not shown), indicating that AdK7 is an excellent vector with high transduction activity and low cytotoxicity in BMSCs.

Efficient osteoblast differentiation in vitro and in vivo by fiber-modified Ad vectors

Because an efficient method for transduction into BMSCs could be established by using AdK7 containing the CA promoter, we expected that efficient differentiation into specialized cells from BMSCs might be achieved by using this Ad vector. To test this, we generated mouse Runx2-expressing Ad vectors, AdK7-CA-Runx2 and Ad-CA-Runx2, because a Runx2 gene is both necessary and sufficient for mesenchymal cell differentiation towards osteoblast lineage [3]. Western blot analysis showed that Runx2 protein levels in AdK7-CA-Runx2-transduced cells were quite higher than those in non-, AdK7-CA-LacZ-, or Ad-CA-Runx2-transduced cells (Fig. 2).

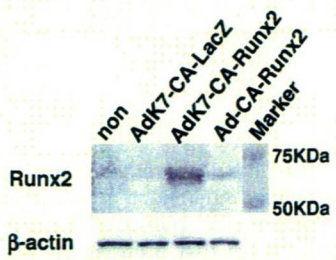

Fig. 2. Runx2 expression in Ad vector-transduced BMSCs. Cell lysates were isolated from BMSCs 2 days after the transduction, and Western blotting was performed.

We next assessed osteoblast differentiation by measuring alkaline phosphatase (ALP) activity, which is a marker of early osteoblast differentiation. After transduction with Ad vector, BMSCs were cultured in osteogenic differentiation medium for the indicated number of days. As shown in Fig. 3A, the ALP activity levels in AdK7-CA-Runx2-transduced cells were extremely increased in comparison with control cells. Notably, AdK7-CA-Runx2 mediated approximately 50-fold higher ALP activity than non-transduction or AdK7-CA-LacZ on day 5 after transduction. These results indicated that early osteoblast differentiation of BMSC was facilitated by AdK7-CA-Runx2. Because mature osteoblasts are known to be specialized in the production of extracellular matrix and the mineralization [22], we next examined the matrix mineralization in BMSCs. von Kossa staining revealed that matrix mineralization in AdK7-CA-Runx2-transduced cells was dramatically increased in comparison with non-, AdK7-CA-LacZ, or Ad-CA-Runx2-transduced cells (Fig. 3B, left). Furthermore, we observed a significant elevation of calcium deposition in AdK7-CA-Runx2-transduced cells even on day 5 after transduction, while neither non-transduced cells nor AdK7-CA-LacZ-transduced cells showed mineralization until day 15 (Fig. 3B, right). Ad-CA-Runx2 mediated slightly higher levels of calcium deposition than non-transduced or AdK7-CA-LacZ-transduced cells, but significantly lower levels than AdK7-CA-Runx2-transduced cells. Additionally, we found that the expression levels of marker genes characteristic of osteoblast differentiation, such as Runx2, osterix, bone sialoprotein, osteocalcin, and type I collagen, were also increased in AdK7-CA-Runx2-transduced cells (Fig. 3C). These results demonstrated that a conventional method using only osteogenic differentiation medium is

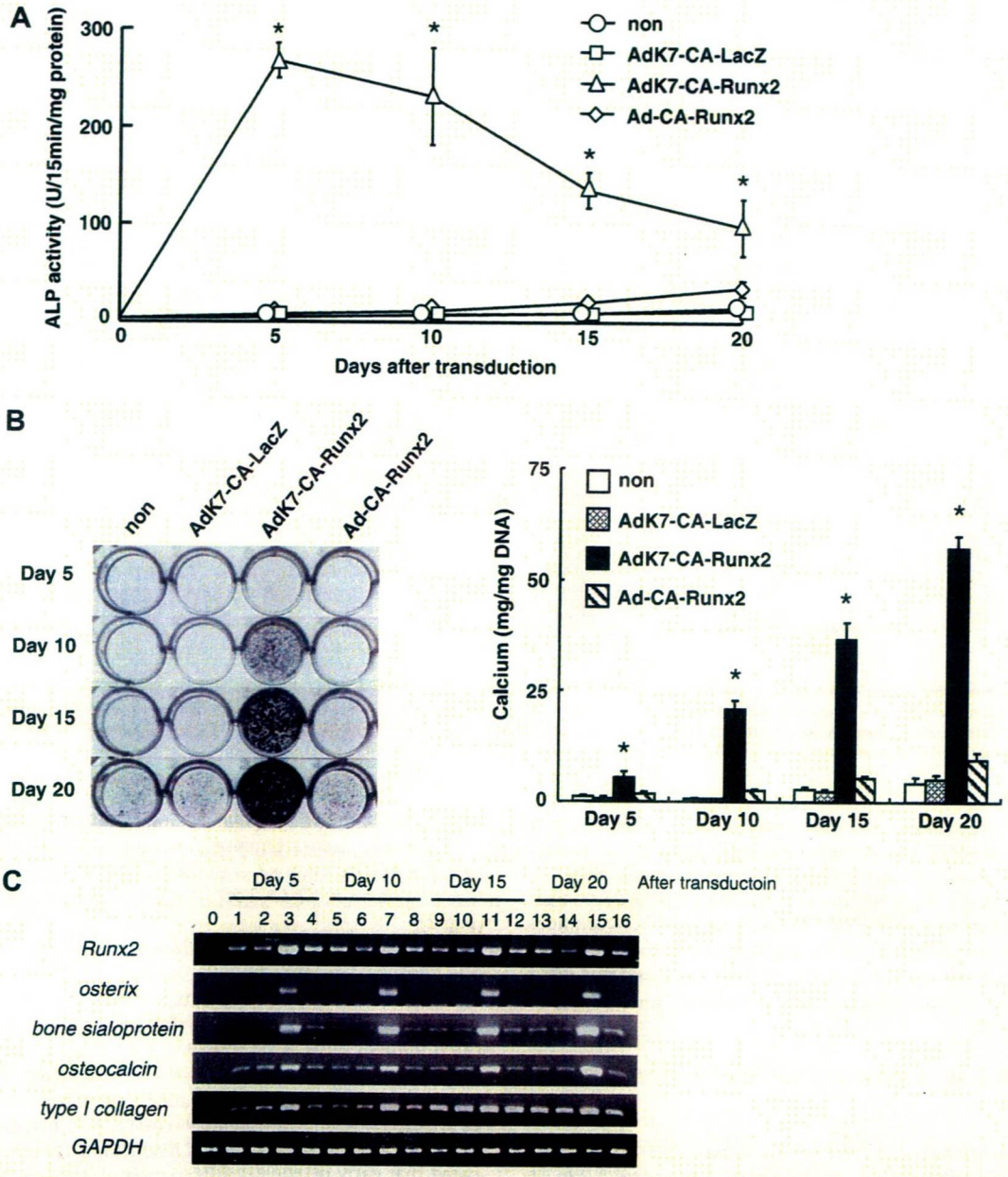

Fig. 3. Promotion of *in vitro* osteoblastic differentiation in AdK7-CA-Runx2-transduced BMSC. After transduction with each Ad vector at 3000 VP/cell for 1.5 hr, BMSCs were cultured for the indicated number of days. (A) ALP activity, (B, left) matrix mineralization, and (B, right) calcium deposition in the cells was determined. The data are expressed as mean ± S.D. ($n = 3$). $p < 0.01$ as compared with non-, AdK7-CA-LacZ-, or Ad-CA-Runx2-transduced cells. (C) RT-PCR was performed using primers for Runx2, osterix, bone sialoprotein, osteocalcin, collagen type I, and GAPDH. Lane 0: non-treated BMSCs; lanes 1, 5, 9, and 13: BMSCs with osteogenic supplements (OS); lanes 2, 6, 10, and 14: BMSCs with OS plus AdK7-CA-LacZ; lanes 3, 7, 11, and 15: BMSCs with OS plus AdK7-CA-Runx2; lanes 4, 8, 12, and 16: BMSCs with OS plus Ad-CA-Runx2.

not enough for efficient osteoblast differentiation, and that, by efficient Runx2 transduction using AdK7, osteoblastogenesis of BMSCs could be dramatically accelerated *in vitro*.

Finally, to examine whether the increased levels of Runx2 expression in BMSCs could enhance the osteogenic potential of BMSC *in vivo*, BMSCs transduced with each Ad vector were injected into the hind limb biceps muscle of nude mice. Microcomputed tomography analysis revealed that no bone formation was observed in non-, AdK7-CA-LacZ-, or Ad-CA-Runx2-transduced cells, while new bone was detected in mice injected with AdK7-CA-Runx2-transduced cells (Fig. 4), indicating that AdK7-CA-Runx2-transduced BMSCs efficiently differentiated into mature osteoblasts *in vivo*. These results clearly showed that AdK7-CA-Runx2 could facilitate the osteogenic potential of BMSCs both *in vitro* and *in vivo*.

Discussion

Because genetic manipulation is considered to be a powerful tool to promote cellular differentiation, it is necessary to establish efficient methods for transduction into BMSCs. Many researchers have reported that transduction efficiency of rat or human MSC was increased by using fiber-modified Ad vectors, such as AdRGD or Ad vectors containing Ad35 fiber knob and

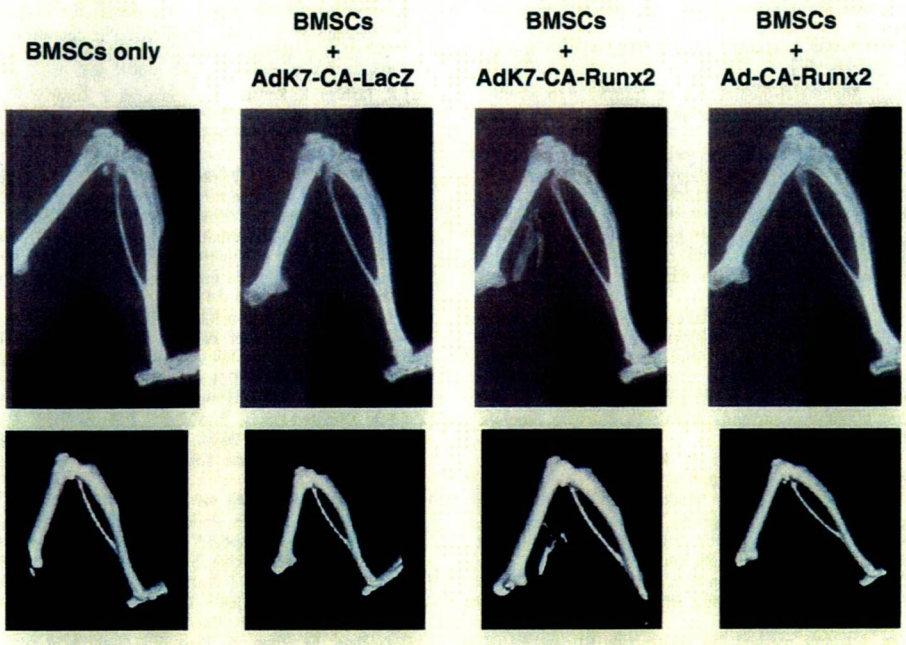

Fig. 4. *In vivo* ectopic bone formation of mouse BMSCs by AdK7-mediated Runx2 gene transduction. BMSCs were transduced with indicated Ad vectors at 3000 VP/cell. On the following day, cells were injected into the hind limb biceps muscle of nude mice. Four weeks later, bone formation was analyzed by the microCT system. Similar results were obtained in two independent experiments. Upper: X-ray images; lower: 3D reconstitution images.

shaft (AdF35) [23–25]. In this study, we demonstrated that AdK7 could express a transgene in BMSCs more efficiently than conventional Ad vector or AdRGD (Fig. 1A and B). Similarly, we have previously shown that the highest transduction efficiency in hMSC could be achieved by using AdK7, but not AdRGD or AdF35 [9]. Therefore, our data indicate that AdK7 is the most appropriate vector for various mesenchymal cells. We also found that the CA promoter showed higher gene expression in BMSCs than did the CMV or EF-1α promoter (Fig. 1C). This appears to be due to the potent activity of the CA promoter in immature cells [18,20]. Hence, we conclude that AdK7 containing the CA promoter is the most suitable vector for transduction into BMSCs.

We demonstrated that osteoblastogenesis of BMSCs was dramatically promoted by using AdK7-mediated Runx2 transduction (Figs. 3 and 4). This is the first study to report the usefulness of AdK7 in the field of stem cell differentiation. Runx2 is known to regulate osteoblastogenesis by controlling the expression of multiple osteoblast marker genes [10]. Because Runx2 protein and mRNA were highly expressed for more than 20 days in AdK7-CA-Runx2-trasduced cells (Figs. 2 and 3C), the expression of marker genes and ALP activity would be increased and would thereby enhance both *in vitro* and *in vivo* osteogenic ability. On the other hand, osteoblast differentiation could not be facilitated by AdK7-CA-Runx2 when osteogenic supplements were removed (data not shown), suggesting that osteogenic supplements were required for matrix mineralization, although differentiation efficiency was low when using only osteogenic supplements. Thus, efficient osteoblast differentiation of BMSCs would be achieved by the synergistic effect of both osteogenic supplements and efficient Runx2 transduction.

Unlike the case with AdK7-CA-Runx2, almost no osteoblast differentiation was seen in Ad-CA-Runx2-transduced cells. However, several groups reported that the osteogenic potential of MSCs was enhanced by Runx2 transduction using the conventional Ad vectors [26,27]. This difference would be attributable to the difference in transduction efficiency in BMSCs using the conventional Ad vector, because they showed that approximately 30–40% of the cells expressed transgenes by conventional Ad vector at 250–500 infectious units (ifu)/cell. Although we could not obtain high transduction efficiency using the conventional Ad vector, we showed that more than 90% of the cells were transduced by using AdK7-CA-LacZ at only 71 ifu/cell (3000 VP/cell) (Fig. 1A), without any decrease in viability (data not shown). Our results indicate that vector doses can be reduced by using AdK7, leading to a decrease in cytotoxicity to the cells. Therefore, AdK7, but not other fiber-modified Ad vectors or conventional Ad vectors, would contribute to safe regenerative medicine procedures.

In summary, we succeeded in developing efficient methods both for transducing mouse BMSCs and differentiating osteoblasts from BMSCs. Recently, many researchers have reported that mesenchymal stem/stromal cells could be isolated from adipose or placental tissues [28,29]. Because these mesenchymal cells are shown to possess mostly the same properties as BMSCs, AdK7 could probably be applied to these cells. Thus, our transduction methods can be a valuable tool for therapeutic applications based on adult mesenchymal stem/stromal cells.

Acknowledgments

We thank Dr. J. Miyazaki and Dr. S. Takeda for providing the CA promoter and the mouse Runx2 cDNA, respectively. This work was supported by grants from the Ministry of Health, Labor, and Welfare of Japan. K.T. is the Research Fellow of the Japan Society for the Promotion of Science.

References

[1] M.F. Pittenger, A.M. Mackay, S.C. Beck, R.K. Jaiswal, R. Douglas, J.D. Mosca, M.A. Moorman, D.W. Simonetti, S. Craig, D.R. Marshak, Multilineage potential of adult human mesenchymal stem cells, Science 284 (1999) 143–147.
[2] M.F. Pittenger, B.J. Martin, Mesenchymal stem cells and their potential as cardiac therapeutics, Circ. Res. 95 (2004) 9–20.

[3] P.J. Marie, Transcription factors controlling osteoblastogenesis, Arch. Biochem. Biophys. 473 (2008) 98–105.
[4] K. Benihoud, P. Yeh, M. Perricaudet, Adenovirus vectors for gene delivery, Curr. Opin. Biotechnol. 10 (1999) 440–447.
[5] P.A. Conget, J.J. Minguell, Adenoviral-mediated gene transfer into ex vivo expanded human bone marrow mesenchymal progenitor cells, Exp. Hematol. 28 (2000) 382–390.
[6] S.C. Hung, C.Y. Lu, S.K. Shyue, H.C. Liu, L.L. Ho, Lineage differentiation-associated loss of adenoviral susceptibility and coxsackie-adenovirus receptor expression in human mesenchymal stem cells, Stem cells 22 (2004) 1321–1329.
[7] I. Dmitriev, V. Krasnykh, C.R. Miller, M. Wang, E. Kashentseva, G. Mikheeva, N. Belousova, D.T. Curiel, An adenovirus vector with genetically modified fibers demonstrates expanded tropism via utilization of a coxsackievirus and adenovirus receptor-independent cell entry mechanism, J. Virol. 72 (1998) 9706–9713.
[8] N. Koizumi, H. Mizuguchi, N. Utoguchi, Y. Watanabe, T. Hayakawa, Generation of fiber-modified adenovirus vectors containing heterologous peptides in both the HI loop and C terminus of the fiber knob, J. Gene Med. 5 (2003) 267–276.
[9] H. Mizuguchi, T. Sasaki, K. Kawabata, F. Sakurai, T. Hayakawa, Fiber-modified adenovirus vectors mediate efficient gene transfer into undifferentiated and adipogenic-differentiated human mesenchymal stem cells, Biochem. Biophys. Res. Commun. 332 (2005) 1101–1106.
[10] P. Ducy, R. Zhang, V. Geoffroy, A.L. Ridall, G. Karsenty, Osf2/Cbfa1: a transcriptional activator of osteoblast differentiation, Cell 89 (1997) 747–754.
[11] T. Komori, H. Yagi, S. Nomura, A. Yamaguchi, K. Sasaki, K. Deguchi, Y. Shimizu, R.T. Bronson, Y.H. Gao, M. Inada, M. Sato, R. Okamoto, Y. Kitamura, S. Yoshiki, T. Kishimoto, Targeted disruption of Cbfa1 results in a complete lack of bone formation owing to maturational arrest of osteoblasts, Cell 89 (1997) 755–764.
[12] H. Mizuguchi, M.A. Kay, Efficient construction of a recombinant adenovirus vector by an improved in vitro ligation method, Hum. Gene Ther. 9 (1998) 2577–2583.
[13] H. Mizuguchi, M.A. Kay, A simple method for constructing E1- and E1/E4-deleted recombinant adenoviral vectors, Hum. Gene Ther. 10 (1999) 2013–2017.
[14] H. Niwa, K. Yamamura, J. Miyazaki, Efficient selection for high-expression transfectants with a novel eukaryotic vector, Gene 108 (1991) 193–199.
[15] K. Kawabata, F. Sakurai, T. Yamaguchi, T. Hayakawa, H. Mizuguchi, Efficient gene transfer into mouse embryonic stem cells with adenovirus vectors, Mol. Ther. 12 (2005) 547–554.
[16] H. Mizuguchi, N. Koizumi, T. Hosono, N. Utoguchi, Y. Watanabe, M.A. Kay, T. Hayakawa, A simplified system for constructing recombinant adenoviral vectors containing heterologous peptides in the HI loop of their fiber knob, Gene Ther. 8 (2001) 730–735.
[17] S. Takeda, J.P. Bonnamy, M.J. Owen, P. Ducy, G. Karsenty, Continuous expression of Cbfa1 in nonhypertrophic chondrocytes uncovers its ability to induce hypertrophic chondrocyte differentiation and partially rescues Cbfa1-deficient mice, Genes Dev. 15 (2001) 467–481.
[18] K. Tashiro, K. Kawabata, H. Sakurai, S. Kurachi, F. Sakurai, K. Yamanishi, H. Mizuguchi, Efficient adenovirus vector-mediated PPAR gamma gene transfer into mouse embryoid bodies promotes adipocyte differentiation, J. Gene Med. 10 (2008) 498–507.
[19] J.V. Maizel Jr., D.O. White, M.D. Scharff, The polypeptides of adenovirus. I. Evidence for multiple protein components in the virion and a comparison of types 2, 7A, and 12, Virology 36 (1968) 115–125.
[20] F. Sakurai, K. Kawabata, T. Yamaguchi, T. Hayakawa, H. Mizuguchi, Optimization of adenovirus serotype 35 vectors for efficient transduction in human hematopoietic progenitors: comparison of promoter activities, Gene Ther. 12 (2005) 1424–1433.
[21] S. Chung, T. Andersson, K.C. Sonntag, L. Bjorklund, O. Isacson, K.S. Kim, Analysis of different promoter systems for efficient transgene expression in mouse embryonic stem cell lines, Stem Cells 20 (2002) 139–145.
[22] H.C. Blair, M. Zaidi, P.H. Schlesinger, Mechanisms balancing skeletal matrix synthesis and degradation, Biochem. J. 364 (2002) 329–341.
[23] E.A. Olmsted-Davis, Z. Gugala, F.H. Gannon, P. Yotnda, R.E. McAlhany, R.W. Lindsey, A.R. Davis, Use of a chimeric adenovirus vector enhances BMP2 production and bone formation, Hum. Gene Ther. 13 (2002) 1337–1347.
[24] S. Knaan-Shanzer, M.J. van de Watering, I. van der Velde, M.A. Goncalves, D. Valerio, A.A. de Vries, Endowing human adenovirus serotype 5 vectors with fiber domains of species B greatly enhances gene transfer into human mesenchymal stem cells, Stem cells 23 (2005) 1598–1607.
[25] H. Tsuda, T. Wada, T. Yamashita, H. Hamada, Enhanced osteoinduction by mesenchymal stem cells transfected with a fiber-mutant adenoviral BMP2 gene, J. Gene Med. 7 (2005) 1322–1334.
[26] Z. Zhao, M. Zhao, G. Xiao, R.T. Franceschi, Gene transfer of the Runx2 transcription factor enhances osteogenic activity of bone marrow stromal cells in vitro and in vivo, Mol. Ther. 12 (2005) 247–253.
[27] X. Zhang, M. Yang, L. Lin, P. Chen, K.T. Ma, C.Y. Zhou, Y.F. Ao, Runx2 overexpression enhances osteoblastic differentiation and mineralization in adipose-derived stem cells in vitro and in vivo, Calcif. Tissue Int. 79 (2006) 169–178.
[28] Y. Fukuchi, H. Nakajima, D. Sugiyama, I. Hirose, T. Kitamura, K. Tsuji, Human placenta-derived cells have mesenchymal stem/progenitor cell potential, Stem Cells 22 (2004) 649–658.
[29] J.M. Gimble, A.J. Katz, B.A. Bunnell, Adipose-derived stem cells for regenerative medicine, Circ. Res. 100 (2007) 1249–1260.

THE JOURNAL OF BIOLOGICAL CHEMISTRY VOL. 285, NO. 20, pp. 15268–15277, May 14, 2010

Pertussis Toxin Up-regulates Angiotensin Type 1 Receptors through Toll-like Receptor 4-mediated Rac Activation*[S]

Received for publication, October 15, 2009, and in revised form, March 8, 2010 Published, JBC Papers in Press, March 15, 2010, DOI 10.1074/jbc.M109.076232

Motohiro Nishida[‡], Reiko Suda[‡], Yuichi Nagamatsu[‡], Shihori Tanabe[§], Naoya Onohara[‡], Michio Nakaya[‡], Yasunori Kanaho[¶], Takahiro Shibata[‖], Koji Uchida[‖], Hideki Sumimoto[**], Yoji Sato[§], and Hitoshi Kurose[‡1]

From the [‡]Department of Pharmacology and Toxicology, Graduate School of Pharmaceutical Sciences, and the [**]Department of Biochemistry, Graduate School of Medical Sciences, Kyushu University, Fukuoka 812-8582, the [§]Division of Cellular and Gene Therapy Products, National Institute of Health Sciences, Setagaya, Tokyo 158-8501, the [¶]Department of Physiological Chemistry, Graduate School of Comprehensive Sciences and Institute of Basic Medical Sciences, University of Tsukuba, Tsukuba 305-8575, and the [‖]Graduate School of Bioagricultural Sciences, Nagoya University, Nagoya 464-8601, Japan

Pertussis toxin (PTX) is recognized as a specific tool that uncouples receptors from G_i and G_o through ADP-ribosylation. During the study analyzing the effects of PTX on Ang II type 1 receptor (AT1R) function in cardiac fibroblasts, we found that PTX increases the number of AT1Rs and enhances AT1R-mediated response. Microarray analysis revealed that PTX increases the induction of interleukin (IL)-1β among cytokines. Inhibition of IL-1β suppressed the enhancement of AT1R-mediated response by PTX. PTX increased the expression of IL-1β and AT1R through NF-κB, and a small GTP-binding protein, Rac, mediated PTX-induced NF-κB activation through NADPH oxidase-dependent production of reactive oxygen species. PTX induced biphasic increases in Rac activity, and the Rac activation in a late but not an early phase was suppressed by IL-1β siRNA, suggesting that IL-1β-induced Rac activation contributes to the amplification of Rac-dependent signaling induced by PTX. Furthermore, inhibition of TLR4 (Toll-like receptor 4) abolished PTX-induced Rac activation and enhancement of AT1R function. However, ADP-ribosylation of G_i/G_o by PTX was not affected by inhibition of TLR4. Thus, PTX binds to two receptors; one is TLR4, which activates Rac, and another is the binding site that is required for ADP-ribosylation of G_i/G_o.

PTX,[2] a major virulence factor of Gram-negative bacillus *Bordetella pertussis*, which causes whooping cough, is well established as a pharmacological tool for a specific inhibitor of G_i signaling. PTX is composed of A-protomer and B-oligomer, and A-protomer exerts ADP-ribosyltransferase activity on the α subunit of heterotrimeric G_i proteins ($G\alpha_i$), leading to inhibition of receptor-G protein coupling (1, 2), whereas B-oligomer of PTX recognizes and binds carbohydrate-containing receptors that deliver A-protomer into the cytosol (3). However, several reports have demonstrated that PTX has additional effects, such as enhancement of immune responses (4–6), increase in adenosine A_1 receptor density (7), and activation of tyrosine kinase, mitogen-activated protein kinase, and NF-κB (8–10). These effects of PTX are reported to be independent of G_i modification.

Angiotensin (Ang) II plays an important role in the regulation of hypertrophy and/or hyperplasia of cardiovascular cells (11–13). In cardiac fibroblasts, Ang II has been demonstrated to stimulate the processes related to extracellular matrix remodeling (14). The biological function of Ang II is mediated by Ang II receptors located on the plasma membrane. Two isoforms (type 1 (AT1) and type 2 (AT2)) of Ang II receptor have been identified, but most of the cardiovascular effects of Ang II are attributed to AT1R (15). AT1R belongs to the G_q-coupled receptor family. Stimulation of AT1R activates phospholipase C and increases $[Ca^{2+}]_i$ through the production of inositol 1,4,5-trisphosphate, leading to the modulation of fibroblast activities, such as cell proliferation and extracellular matrix protein synthesis (16).

An increase in AT1R density is one of the features to enhance fibrogenic responses of the heart. For example, an increase in AT1R density has been reported in the heart after myocardial infarction (17, 18) and in hearts from biopsies from patients with spontaneous intracerebral hemorrhage (19). Several cytokines, such as tumor necrosis factor (TNF)-α and interleukin (IL)-1β, have been reported to up-regulate AT1R (17, 20). However, the molecular mechanism responsible for the increase in AT1R density is still unknown.

Many studies suggest that low concentration of ROS acts as a second messenger in the cardiovascular system (21, 22). Stimulation of IL-1β and TNF-α induces ROS production through

* This work was supported by grants from the Ministry of Education, Culture, Sports, Science, and Technology of Japan (to M. Nishida, M. Nakaya, and H. K.); a grant-in-aid for scientific research on Innovative Areas (to M. Nishida); a grant-in-aid for scientific research on Priority Areas (to H. K.); and grants from the Nakatomi Foundation, Sapporo Bioscience Foundation, and Naito Foundation (to M. Nishida).

[S] The on-line version of this article (available at http://www.jbc.org) contains supplemental Tables 1 and 2 and Figs. 1–4.

The data discussed in this study have been deposited in the NCBI Gene Expression Omnibus (GEO) (http://www.ncbi.nlm.nih.gov/geo) and are accessible through GEO Series accession number GSE5017.

[1] To whom correspondence should be addressed. Tel./Fax: 81-92-642-6884; E-mail: kurose@phar.kyushu-u.ac.jp.

[2] The abbreviations used are: PTX, pertussis toxin; Ang II, angiotensin II; AT1R, Ang II type 1 receptor; DN-Rac and DN-p47^{phox}, dominant negative Rac and p47^{phox}, respectively; DPI, diphenyleneiodonium; GFP, green fluorescent protein; ct, carboxyl terminal region; IκBαm, non-phosphorylated form of IκBα, which works as a dominant negative mutant; IL, interleukin; MOI, multiplicity of infection; NF-κB, nuclear factor κB; IκB, inhibitor of κB; PH, pleckstrin homology; PI, phosphatidylinositol; PI-3-P, PI 3-phosphate; PLC, phospholipase C; PX, *phox* homology; Ro-106-9920, 6-(phenylsulfinyl)tetrazolo[1,5-*b*]pyridazine; ROS, reactive oxygen species; TNF-α, tumor necrosis factor-α; WT, wild type; ELISA, enzyme-linked immunosorbent assay; siRNA, small interfering RNA.

NADPH oxidase activation (23). A small GTP-binding protein, Rac, regulates the activity of NADPH oxidase (24) and mediates IL-1β- or TNF-α-induced ROS production and NF-κB activation (25). We have previously reported that Rac mediates Ang II-stimulated ROS production through NADPH oxidase activation in cardiac myocytes and cardiac fibroblasts (26, 27). Overexpression of constitutively active Rac1 induces hypertrophic responses in isolated cardiomyocyte and dilated cardiomyopathy *in vivo* (28, 29). Although a high concentration of hydrogen peroxide (H_2O_2) is reported to decrease AT1R density (30), it is unknown whether production of low concentration of ROS via Rac-mediated NADPH oxidase activation participates in the receptor-stimulated increase in AT1R density of cardiac cells.

Toll-like receptors (TLRs) play a critical role in both innate and adaptive immunity (31). There are at least 10 TLRs identified so far in humans, which specifically recognize and bind to a variety of pathogenic factors, including lipopolysaccharide. The mouse heart expresses at least six receptors (TLR2, -3, -4, -5, -7, and -9), and the stimulation of these receptors induces activation of NF-κB. TLR2 and TLR4 have been extensively studied in the heart, and both receptors are in part responsible for cardiac dysfunction in certain pathological conditions (32). Recent studies have elucidated that PTX functions as a superior ligand for TLR4 (6, 10). Although stimulation of TLR4 results in production of proinflammatory cytokines, it has not been reported that PTX exerts some pharmacological action(s) through TLR4 in cardiovascular cells, and it is unknown whether PTX-induced ADP-ribosylation of G_i/G_o requires TLR4-mediated entry into cells.

During the study of the role of G_i proteins in AT1R-mediated fibrotic responses using rat neonatal cardiac fibroblasts, we found that PTX enhances Ang II-induced increase in $[Ca^{2+}]_i$. Because we previously reported that the treatment with PTX increases Rac activity in rat neonatal cardiac myocytes (26), we hypothesized that Rac is implicated in PTX-induced enhancement of Ang II signaling in cardiac fibroblasts. In this study, we demonstrate that PTX B-oligomer induces Rac activation through a pathway independent of ADP-ribosylation of G_i/G_o. PTX increases IL-1β induction through sequential activation of TLR4, Rac, NADPH oxidase, and NF-κB, which leads to AT1R up-regulation through amplification of Rac-dependent signaling in rat cardiac fibroblasts.

EXPERIMENTAL PROCEDURES

Materials, Recombinant Adenoviruses, and Culture of Cardiac Fibroblasts—PTX, simvastatin, and anti-$G\alpha_{q/11}$ antibody were purchased from Calbiochem. Ang II was from Peptide Institute. Mastparan-7, ATP, wortmannin, and diphenyleneiodonium (DPI) were purchased from Sigma. Ro-106-9920 was from Tocris. Rat IL-1β and PTX B-oligomer were from Wako. Rabbit anti-rat IL-1β antibody and the rat IL-1β ELISA kit were from Endogen. Anti-$G\alpha_{11}$, anti-$PLC\beta_3$, anti-IκBα, anti-p65, anti-RhoA, anti-rabbit IgG, and anti-mouse IgG antibodies were purchased from Santa Cruz Biotechnology, Inc. (Santa Cruz, CA). [^{125}I]Ang II, [^{32}P]NAD, and glutathione-Sepharose beads were from Amersham Biosciences. Anti-Rac1 and anti-Rap1 antibodies were from Transduction Laboratories. Anti-Ras antibody was from Upstate Biotechnology. Anti-phospho-Akt and anti-Akt antibodies were from Cell Signaling. Fura2/AM was from Dojindo. 2,7-dichlorofluorescein diacetate and Alexa Fluor 488 goat anti-rabbit antibody were from Molecular Probes. Collagenase and Fugene 6 were from Roche Applied Science. Dual luciferase reagents were from Promega. pNF-κB-Luc and pRL-SV40 were from Stratagene. The sequences coding the Rap1-binding domain of Ral-GDS, Rac-binding domain of p21-activated kinase, Rho-binding domain of rhotekin, or Ras-binding domain of Raf were cloned, sequenced, and ligated into pGEX-4T-1 to make glutathione *S*-transferase fusion protein constructs. Glutathione *S*-transferase fusion proteins were expressed at room temperature and purified using gluthathione-Sepharose as described (33). The cDNA encoding GRP1-PH was provided by Dr. Alexander Gray (University of Dundee, Scotland). Recombinant adenoviruses of GRK2 (G protein-coupled receptor kinase 2)-ct, RGS4 (regulator of G protein signaling 4), WT $G\alpha_i$, $G\alpha_i$-ct, IκBαm, GFP-fused WT Rac, GFP-fused constitutively active Rac (G12V), DN-Rac (T17N), DN-$p47^{phox}$, and p115-RGS were produced as described previously (26, 34). Stealth siRNAs oligonucleotides for rat IL-1β, TLR4, and Rac1 were from Invitrogen. Sequences of stealth siRNA used were described in supplemental Table 1. Cardiac fibroblasts were prepared from ventricles of 1–2-day-old Sprague-Dawley rats, as described previously (27).

Quantification of Intracellular Ca^{2+} and ROS Concentration—$[Ca^{2+}]^i$ was measured by the method described previously (35). Briefly, cells (5×10^4) were plated on a 3 × 10-mm microcoverglass (MATSUNAMI) and loaded with 1 μM fura-2/AM in the cultured medium at 37 °C for 30 min. Cells were washed with HEPES-buffered salt solution containing 107 mM NaCl, 6 mM KCl, 1.2 mM $MgSO_4$, 0.5 mM EGTA, 20 mM HEPES (pH 7.4), and 11.5 mM glucose. Measurement of intracellular ROS concentration was performed in 2 mM Ca^{2+}-containing HEPES-buffered salt solution with a fluorescent dye, 2,7-dichlorofluorescein diacetate, as described previously (27). Fluorescence images were recorded and analyzed with a video image analysis system (Aquacosmos, Hamamatsu Photonics). The peak changes ($\Delta F/F_0$) of dichlorofluorescein fluorescence intensity were identified as values obtained by subtracting the basal fluorescence intensity (F_0) from the maximal intensity during a 15-min PTX treatment.

Measurement of IL-1β mRNA and Protein Expression—Expression of IL-1β mRNA and protein was measured by real time reverse transcription-PCR and ELISA, as described previously (36). For the preparation of real time reverse transcription-PCR analysis, cells (3×10^5) plated on 6-well dishes were treated with PTX for 24 h and lysed with 400 μl of RLT buffer (Qiagen). For ELISA, cells (1×10^5) on 12-well dishes were treated with PTX (100 ng/ml) in 500 μl of medium, and cells were then collected together with medium. After cells were homogenized with a 26-gauge syringe, 100 μl of supernatants were used. Assays were performed according to the manufacturer's instructions.

Microarray Analysis—Cells (1×10^6) plated on 35-mm dishes were treated with PTX for 24 h and lysed with 400 μl of RLT buffer. Total RNA was extracted with the RNeasy minikit (Qiagen) and RNase-free DNase set (Qiagen). Total RNA was converted to biotin-labeled cRNA, which was hybridized to the

rat genome U34A GeneChip (Affymetrix) for 16–24 h at 45 °C. The hybridization signals on the microarray were scanned and computed at a target intensity of 500 by a GeneChip Scanner 3000 and GeneChip Operating Software (Affymetrix), respectively. The data analysis was performed as follows. At the first step, probe sets without expression in the fibroblasts, which were indicated as absent by absolute analysis in more than half of the replicates in both the control and PTX-treated groups, were eliminated from the data set. Then, if the difference in the mean signal intensity of a given probe set was equal to the cut-off (1.25-fold) or more between the control and PTX-treated groups and if its p value calculated by Student's t test was less than 0.05, that probe set was employed. At the last step, probe sets with an annotation "signal transduction" (GO:0007165) in the AmiGO data base (available on the World Wide Web) were extracted, using the NetAffx Gene Ontology Mining Tool (available on the World Wide Web).

Ang II Binding Assay—Measurement of Ang receptor binding was performed according to the previous report (15) with a slight modification. After various treatments for 24 h, cardiac fibroblasts were rinsed with 10 ml of ice-cold phosphate-buffered saline and mechanically detached in 1 ml of ice-cold lysis buffer containing 10 mM Tris, pH 7.4, 5 mM EDTA, 5 mM EGTA, 1 μg/ml benzamidine, 10 μg/ml soybean trypsin inhibitor (type II-S), and 5 μg/ml leupeptin. The cell lysate was centrifuged at 45,000 × g for 10 min at 4 °C. The pellet containing crude membrane fraction was resuspended in 1 ml of ice-cold lysis buffer with a Potter type homogenizer, frozen, and stored at −80 °C until use. After the concentration of membrane protein was determined, membrane protein (20 μg) was used for the binding studies. The membrane was incubated with 0.1 nM ^{125}I-Ang II in 75 mM Tris, pH 7.4, 12.5 mM $MgCl_2$, 2 mM EDTA, and increasing concentrations of unlabeled Ang II (0–14 nM) for 1 h at 25 °C. Nonspecific binding was determined in the presence of 1 μM unlabeled Ang II. The reaction mixture was filtered over Whatman GF/C filters. The filters were washed with ice-cold buffer containing 25 mM Tris, pH 7.4, and 1 mM $MgCl_2$. The bound ^{125}I-Ang II on the filters was measured with a γ-counter. The values of K_d and B_{max} were calculated by Prism software (GraphPad Software, San Diego, CA).

Measurement of NF-κB Activity—After adenovirus was infected at 100 MOI for 2 h in serum-free medium, fibroblasts (3×10^5 cells) in a 24-well plate were transiently co-transfected with 0.45 μg of pNF-κB-Luc and 0.05 μg of pRL-SV40 control plasmid, using Fugene 6 (27). Luciferase activity was measured 48 h after transfection with dual luciferase reagents.

Measurement of Small GTPase Activities—Activation of small G proteins was determined as described previously (26). Activated Rac, Rho, Ras, and Rap1 were pulled down with 5 μg of glutathione S-transferase-fused Rac-interacting domain of p21-activated kinase (PAK-CRIB), Rho-binding domain of rhotekin (34), Ras-binding domain of Raf-1 (37), and Rap1-binding domain of Ral-GDS (38), respectively. Pulled-down small G proteins were detected with anti-Rac1, anti-RhoA, anti-Ras and anti-Rap1 antibodies. For knockdown of Rac1, cells were transfected with a mixture of Rac1 siRNAs (50 nM each) for 72 h.

Confocal Visualization of GFP-fused Proteins and NF-κB p65 Subunit—Cells (1×10^5) plated on glass bottom 35-mm dishes were infected for 24 h with GFP, GFP-Rac, GFP-constitutively active Rac, GFP fusion protein with PX domain of $p40^{phox}$ ($p40^{phox}$-PX), and $p40^{phox}$-PX (R105K). After the treatment with PTX (100 ng/ml) for 24 h, cells were fixed by 10% formaldehyde neutral buffer solution. For localization of NF-κB, cells were stained with anti-p65 antibody. Fluorescence images were measured at an excitation wavelength of 488 nm with a laser-scanning confocal imaging system (Carl Zeiss LSM510).

In Vitro PTX-catalyzed ADP-ribosylation Assay—*In vitro* ADP-ribosylation of $G\alpha_i$ proteins by PTX was performed as described previously (39) with a slight modification. Briefly, cardiac fibroblasts pretreated with or without 100 ng/ml PTX for 24 h were harvested with ice-cold lysis buffer containing 50 mM Tris (pH 7.5), 5 mM EDTA, 5 mM EGTA, 10 μg/ml benzamidine, 5 μg/ml aprotinin, and 5 μg/ml leupeptin. After centrifugation at 15,000 rpm for 10 min at 4 °C, the pellet was resuspended in lysis buffer. PTX was preactivated by incubation in the solution containing 50 mM Tris (pH 7.5), 5 mM ATP, 20 mM dithiothreitol, and 1 mg/ml bovine serum albumin for 30 min at 30 °C. Then activated PTX was added to the assay mixture, including 100 μg of the membrane, and incubated for 60 min at 30 °C. The final concentrations of all reagents in the assay mixture were as follows: 50 mM Tris (pH 7.5), 50 μM GDP, 10 mM thymidine, 5 μM NAD, 0.5 μM [^{32}P]NAD, 20 μg/ml PTX, 0.2 mg/ml bovine serum albumin, 1 mM ATP, and 4 mM dithiothreitol. The reaction was stopped by the addition of an excessive amount of ice-cold 50 mM Tris (pH 7.5), and the samples were centrifuged at 15,000 rpm for 10 min at 4 °C. The pellet was solubilized in SDS sample buffer, boiled, and subjected to 12% SDS-PAGE. Radioactive bands were detected by filmless autoradiographic analysis (BAS2000 system, Fujifilm).

Statistical Analysis—The results are presented as mean ± S.E. from at least three independent experiments. The representative data of time course experiments were plotted from one of three similar experiments that were performed with more than 20 cells. The mean values were compared with control by one-way analysis followed by Dunnet's t test (for three or more groups) or Student's t test (for two groups).

RESULTS

PTX Enhances Ang II-induced Ca^{2+} Release through AT1R Up-regulation—During the study of AT1R function in cardiac fibroblasts, we found that treatment with PTX enhances transient increase in $[Ca^{2+}]_i$ induced by Ang II at low concentration in the absence of extracellular Ca^{2+} (Fig. 1*A*). The EC_{50} value of Ang II for the changes in $[Ca^{2+}]_i$ increases was 464 ± 44 pM in control cells, whereas the EC_{50} value was decreased to 91 ± 33 pM in PTX-pretreated cells (Fig. 1*B*). However, the ATP-induced Ca^{2+} release was not affected by PTX (Fig. 1*C*). These results suggest that PTX selectively enhances Ca^{2+} response induced by AT1R stimulation. We also found that treatment with PTX for 24 h resulted in a 2-fold increase in maximal ^{125}I-Ang II binding activity (B_{max}) in comparison with PTX-untreated membrane (Fig. 1*D*). PTX increased AT1R density in a time-dependent manner, and more than 18 h was required for a 2-fold increase in AT1R density (supplemental Fig. 1). The

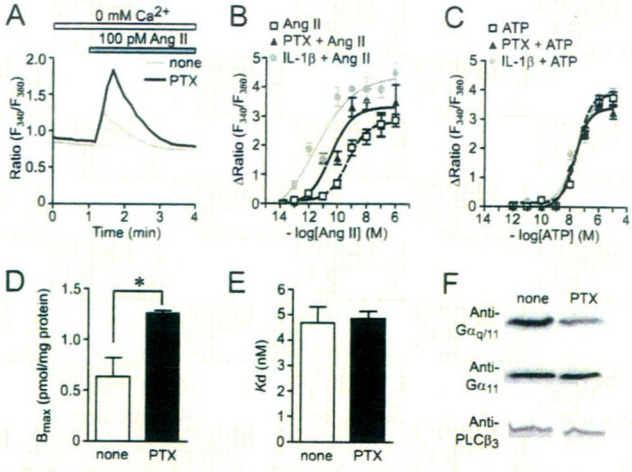

FIGURE 1. **PTX enhances Ca^{2+} responses by Ang II through AT1R up-regulation.** *A*, average time courses of Ca^{2+} response induced by Ang receptor stimulation with Ang II (100 pM) in control and PTX-treated cells. *B* and *C*, peak increases in $[Ca^{2+}]_i$ ($\Delta Ratio$) plotted against various concentrations of Ang II (*B*) and ATP (*C*) in control, PTX-treated, and IL-1β-treated cells. Cells were treated with PTX (100 ng/ml) or IL-1β (10 ng/ml) for 24 h before agonist stimulation. *D* and *E*, increases in AT1R density induced by PTX (100 ng/ml) for 24 h. The B_{max} (*D*) and K_d (*E*) values for Ang II binding were calculated with GraphPad Prism software. *F*, effects of PTX on expression of $G\alpha_{q/11}$ and PLCβ_3. *, $p < 0.05$ *versus* PTX-untreated cells. *Error bars*, S.E.

PTX-induced increase in B_{max} was completely suppressed by CV11974 (1 μM, AT1R-selective blocker) but not by PD123319 (1 μM, AT2R-selective blocker) (data not shown). The K_d value was not affected by PTX (Fig. 1*E*), indicating that the PTX-induced enhancement of AT1R function is not explained by structural changes in AT1R. It has been reported that the increased expression of $G\alpha_{q/11}$ and PLCβ_3 is involved in the enhancement of Ang II-induced Ca^{2+} responses in the ischemic heart (40, 41). However, PTX did not affect the expression levels of $G\alpha_q$, $G\alpha_{11}$, and PLCβ_3 (Fig. 1*F*). These results suggest that the enhancement of Ang II-induced Ca^{2+} release in PTX-treated cells is due to AT1R up-regulation but not up-regulation of components of the $G\alpha_q$-PLCβ pathway.

Because commercially available PTX contaminates with other endotoxins, including lipopolysaccharide, it is possible that other endotoxins contribute to enhancement of AT1R function. Thus, we examined the effects of denatured PTX or PTX purchased from another manufacturer (Sigma) on AT1R functions. Pretreatment of PTX with heat significantly reduced the enhancement of Ang II-induced Ca^{2+} release induced by PTX (supplemental Fig. 1). In contrast, the Ang II-induced Ca^{2+} release was also enhanced by PTX purchased from Sigma as well as that induced by PTX from Calbiochem. These results suggest that PTX proteins *per se* induce AT1R up-regulation in cardiac fibroblasts.

IL-1β Production Induced by PTX Treatment—To examine whether PTX treatment induces production of a factor(s) that participates in up-regulation of AT1R, we performed microarray analysis of mRNAs from PTX-treated fibroblasts. For each gene, we calculated the average intensity in expression for both control and PTX-treated cells and plotted the ratio of these two induction values. Genes were chosen whose expression was at least 1.25-fold increased or decreased as compared with control cells. The probe sets of 405 genes showed significant changes by PTX treatment. Genes were then assigned to several groups according to their function, and we picked out 70 genes in the gene cluster that is termed "signal transduction" in the AmiGO data base (supplemental Table 2). PTX treatment selectively increased AT1R mRNA (Fig. 2*A*) but not other G protein-coupled receptors. Among genes increased by PTX treatment, IL-1α and IL-1β mRNAs showed a marked increase in expression (Fig. 2*A*). Real-time PCR confirmed the strong induction of IL-1β mRNA by PTX treatment (Fig. 2*B*). Although PTX is reported to increase IL-12 expression by inhibition of G_i signaling in T lymphocytes (42), PTX did not significantly increase mRNA expression of other cytokines (supplemental Table 1). Treatment with mastoparan-7 or the expression of WT $G\alpha_i$ or inhibitory polypeptides of G_i signaling ($G\alpha_i$-ct, a polypeptide that specifically inhibits receptor-G_i protein coupling (39); RGS4, a GTPase-activating protein that specifically binds the GTP-bound form of $G\alpha_i$ and $G\alpha_q$ (43); and GRK2-ct, a G$\beta\gamma$ ($\beta\gamma$ subunit of heterotrimeric G protein)-sequestering polypeptide (44)) did not increase IL-1β mRNA expression (Fig. 2*B*). We also confirmed that the expression of $G\alpha_i$-ct did not enhance Ang II-induced Ca^{2+} release (data not shown), and the treatment with B-oligomer of PTX enhanced Ang II-induced Ca^{2+} release (Fig. 2*C*). Furthermore, ELISA revealed that the treatment with PTX actually increased the expression of IL-1β protein levels, whereas the expression of IL-1α protein was below the detection level in PTX-treated cardiac fibroblasts (Fig. 2*D*). These results suggest that PTX selectively induces IL-1β production, and G_i modification is not required for PTX-induced IL-1β production.

IL-1β Mediates PTX-induced Enhancement of Ang II-induced Ca^{2+} Response—Because it has been reported that IL-1β increases AT1R density in cardiac fibroblasts (17, 45), the cells were treated with IL-1β. Treatment with IL-1β (10 ng/ml) enhanced Ang II-induced Ca^{2+} release ($EC_{50} = 31 \pm 26$ pM) but not ATP-induced Ca^{2+} release, in rat cardiac fibroblasts (Fig. 1, *B* and *C*). These effects of IL-1β are similar to the effects of PTX treatment, and the enhancement by IL-1β seems to be consistent with the findings that PTX treatment increased the induction of IL-1β mRNA and protein. Thus, we examined whether PTX-induced IL-1β production participates in the enhancement of AT1R function. The PTX-induced IL-1β production was suppressed by the treatment with IL-1β siRNAs (Fig. 2*E*). The enhancement of Ang II-induced Ca^{2+} release by IL-1β treatment was almost completely suppressed by anti-IL-1β neutral antibody (Fig. 2*F*), indicating that the antibody sufficiently inhibits IL-1β-mediated responses. The enhancement of Ang II-induced Ca^{2+} release by PTX was also suppressed by anti-IL-1β antibody and IL-1β siRNAs (Fig. 2*G*), indicating that PTX-induced IL-1β secretion mediates the enhancement of Ang II-induced Ca^{2+} release.

Involvement of NF-κB in PTX-induced IL-1β Expression—As the promoter regions of IL-1β and AT1R contain a putative NF-κB binding site (46–48), we next examined the involvement of NF-κB in PTX-induced IL-1β production. As shown in Fig. 3*A*, PTX-induced increase in IL-1β mRNA expression was suppressed by the treatment with Ro-106-9920, a selective inhibitor of IκB phosphorylation, and by the expression of a dominant negative IκB, IκBαm. Because Ro-106-9920 showed

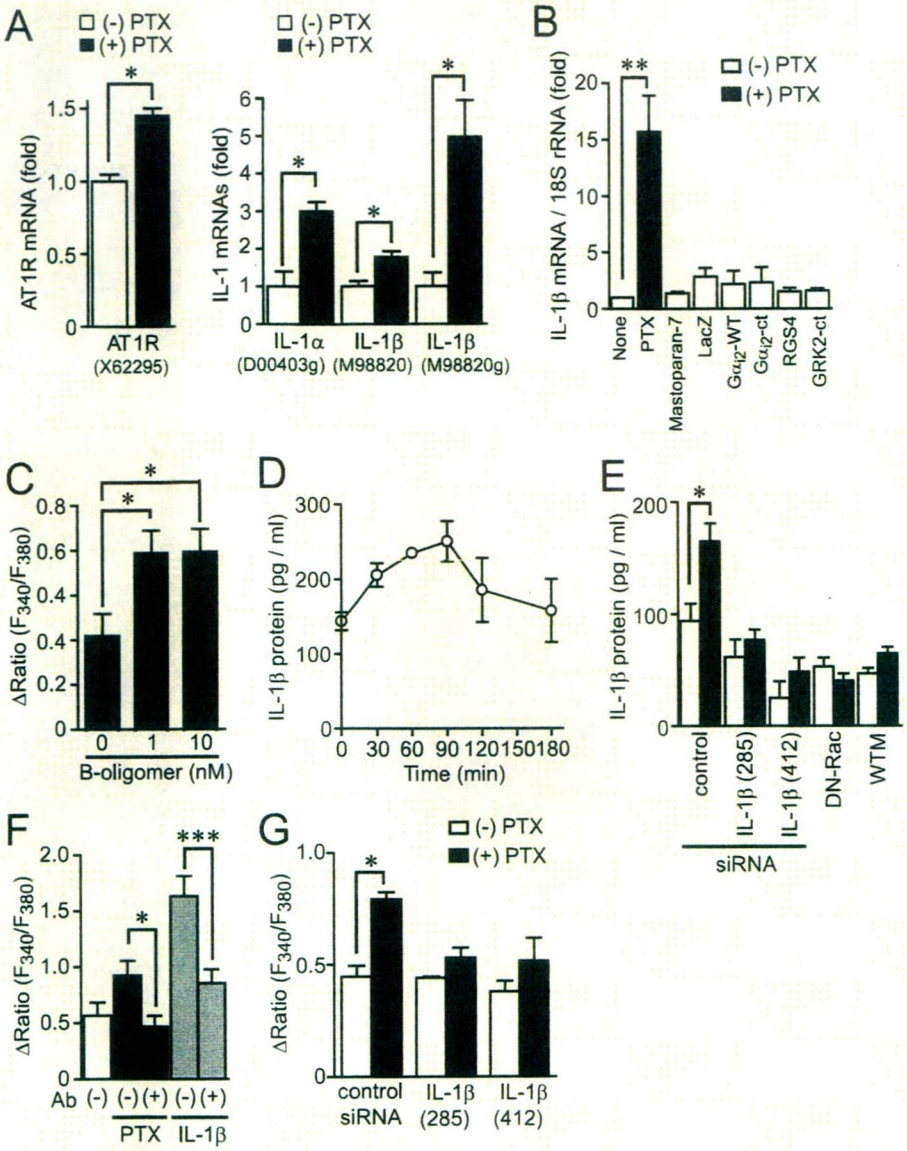

FIGURE 2. **Involvement of IL-1β production in PTX-induced enhancement of Ca^{2+} response by Ang II stimulation.** *A*, effects of PTX on the expression of AT1R, IL-1α, and IL-1β mRNAs. After cells were treated with PTX (100 ng/ml) for 24 h, total RNA was extracted. The expression of mRNAs was determined with microarray analysis. ID numbers of primer probe sets are shown in *parenthesis*. *B*, effects of respective reagents on IL-1β mRNA expression in cardiac fibroblasts. Cells were treated with PTX (100 ng/ml) for 24 h, treated with mastoparan-7 (10 μM) for 12 h, or infected with LacZ, WT $Gα_i$, $Gα_i$-ct, RGS4, and GRK2-ct at 300 MOI for 48 h. The -fold increases were calculated by the values of untreated cells (none) set as 1. *C*, effects of B-oligomer of PTX on Ang II-induced Ca^{2+} releases. Cells were treated with B-oligomer (1 or 10 nM) for 24 h before Ca^{2+} measurement. *D*, time course of PTX-induced expression of IL-1β protein. *E*, effects of IL-1β siRNAs, DN-Rac, and wortmannin (*WTM*) on PTX-induced IL-1β production. Two different siRNAs were used. *F* and *G*, effects of IL-1β neutral antibody (*F*) or IL-1β siRNAs (*G*) on Ang II-induced Ca^{2+} responses in control, PTX-treated, or IL-1β-treated cells. Cells were treated with PTX (100 ng/ml) or IL-1β (1 ng/ml) for 24 h before Ang II (100 pM) stimulation with or without anti-IL-1β antibody (500 μg/ml). Cells were transfected with IL-1β siRNAs (100 nM) 48 h before PTX treatment. *, $p < 0.05$; **, $p < 0.01$; ***, $p < 0.001$ *versus* PTX-untreated, B-oligomer-untreated, control siRNA-treated, PTX-treated, or IL-1β-treated cells. *Error bars*, S.E.

cytotoxic effects at higher concentration, we could not increase the concentration to observe complete inhibition of the IL-1β induction. The enhancement of AT1R function by PTX was suppressed by Ro-106-9920 and IκBαm (Fig. 3*B*), and the PTX-induced increase in AT1R density was suppressed by IκBαm (Fig. 3, *C* and *D*). Because an inhibition of NADPH oxidase activity suppresses NF-κB activation and IL-1β production induced by $Gα_{13}$ activation (36), we next examined the involvement of NADPH oxidase. Treatment with PTX increased NF-κB-dependent luciferase activity (Fig. 3, *E* and *F*). This NF-κB activation was suppressed by the treatment with DPI or by the expression of dominant negative (DN)-Rac and DN-$p47^{phox}$, both of which are essential for NADPH oxidase activation (24), but not by p115-RGS, a $Gα_{13}$-inhibitory polypeptide (26). These results suggest that PTX induces NF-κB activation through Rac-NADPH oxidase pathway and that NF-κB mediates PTX-induced IL-1β production and AT1R up-regulation.

Rac Mediates PTX-induced IL-1β Production and AT1R Up-regulation—We have previously reported in rat neonatal cardiomyocytes that PTX increases basal Rac activity (26). Because the PTX-induced NF-κB activation and IL-1β production was suppressed by DN-Rac (Figs. 2 and 3), we next examined whether PTX increases Rac activity in cardiac fibroblasts. Rac was activated from 10 min after PTX treatment and still activated at 24 h after the treatment (Fig. 4*A*). We also found that PTX did not affect the activities of other small G proteins, Ras, Rap1, and RhoA (supplemental Fig. 2). It has been reported that phosphatidylinositol (PI) 3-kinase participates in PTX B-oligomer-induced antiapoptotic action against HIV-Tat infection in NK cells (49). We confirmed that PTX B-oligomer increased Rac activity in cardiac fibroblasts (supplemental Fig. 3). Pretreatment with wortmannin completely suppressed PTX-induced Rac activation (Fig. 4*B*). The activated Rac has been reported to translocate from cytosol to the plasma membrane through recognition of membrane phospholipids, such as PI 3-phosphate (PI-3-P), PI 4-phosphate, PI 5-phosphate, and PI 3,4,5-trisphosphate, through the carboxyl-terminal polybasic region of Rac (50–52). Confocal imaging revealed that PTX actually translocated GFP-fused WT Rac from cytosol to the plasma membrane, as observed with constitutively active Rac (Fig. 4*C*). Pretreatment with wortmannin inhibited PTX-induced membrane localization of Rac. To demonstrate the involvement of PI-3-P, $p40^{phox}$-

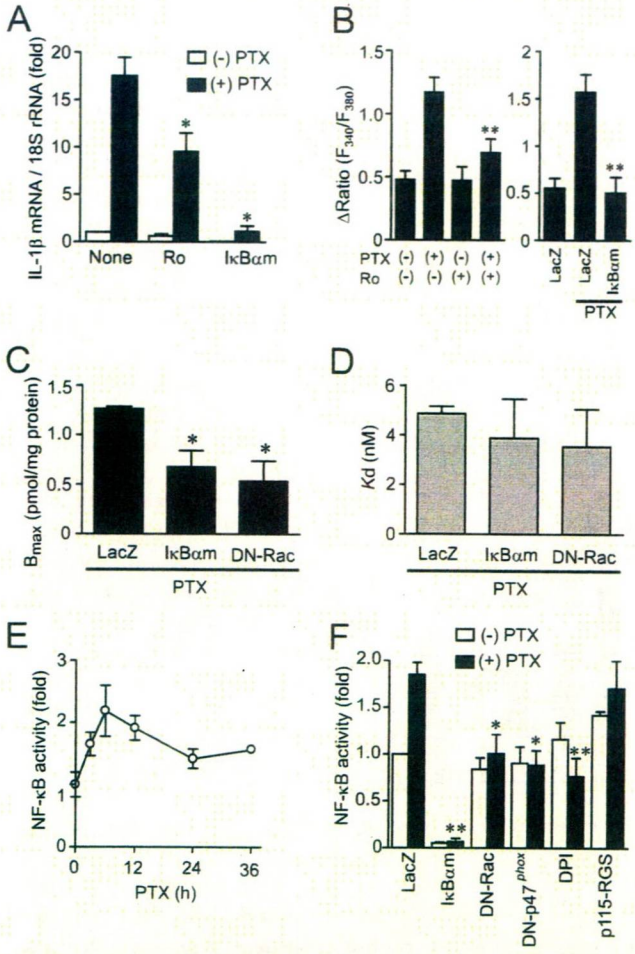

FIGURE 3. **Requirement of NF-κB for PTX-induced enhancement of Ca^{2+} response by Ang II stimulation.** *A*, effects of Ro106-9920 and IκBαm on PTX-induced IL-1β mRNA expression. Cells were pretreated for 20 min with Ro106-9920 (1 μM) or infected with IκBαm (100 MOI) for 48 h before the treatment of PTX (100 ng/ml) for 24 h. *B*, effects of NF-κB inhibitors on Ang II-induced Ca^{2+} responses in PTX-treated cells. *C* and *D*, effects of IκBαm and DN-Rac on PTX-induced increase in AT1R density. Cells were infected with adenoviruses expressing IκBαm or DN-Rac 24 h before PTX treatment. AT1R density was determined with receptor binding assay. *E*, time course of PTX-induced changes in NF-κB-dependent luciferase activity. *F*, effects of IκBαm, DN-Rac, DN-$p47^{phox}$, DPI, and p115-RGS on PTX-induced NF-κB activation. Cells were infected with LacZ, IκBαm, DN-Rac, DN-$p47^{phox}$, or p115-RGS at 100 MOI for 48 h or pretreated with DPI (5 μM) for 20 min before the addition of PTX (100 ng/ml) for 6 h. *, $p < 0.05$; **, $p < 0.01$ *versus* PTX-untreated or LacZ-expressing cells. *Error bars*, S.E.

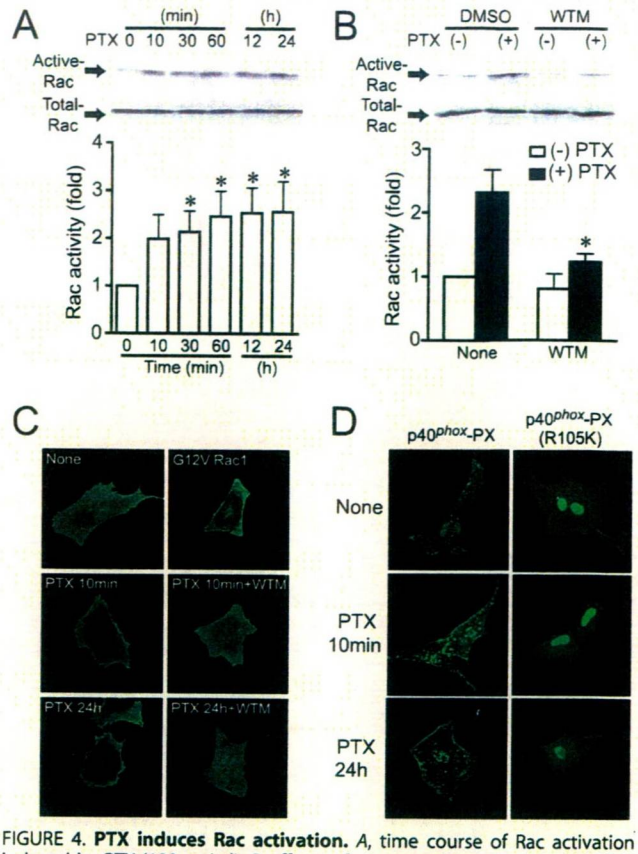

FIGURE 4. **PTX induces Rac activation.** *A*, time course of Rac activation induced by PTX (100 ng/ml). *B*, effects of wortmannin on PTX-induced Rac activation. Cells were pretreated with wortmannin (*WTM*; 100 nM) for 10 min before PTX stimulation. *C*, localization of GFP-fused wild type Rac and constitutively active Rac (*CA-Rac*) (G12V) with or without PTX stimulation. *D*, localization of GFP-fused PX domain of $p40^{phox}$ ($p40^{phox}$-PX), and PI-3-P interaction-deficient mutant ($p40^{phox}$-PX (R105K)) with or without PTX treatment. *, $p < 0.05$ *versus* PTX-untreated cells. *Error bars*, S.E.

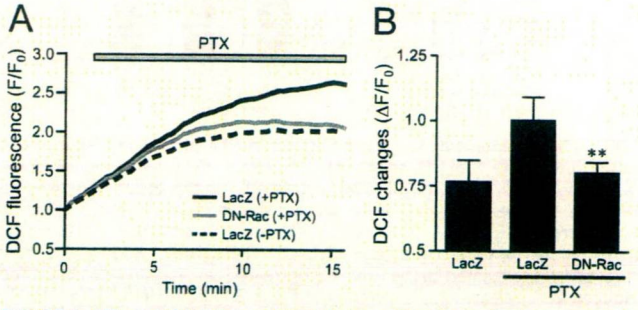

FIGURE 5. **Effects of DN-Rac on PTX-induced ROS production.** *A* and *B*, average changes (*A*) and peak increases (*B*) in PTX-induced F/F_0 of dichlorofluorescein from time course experiments. The increases in PTX-induced fluorescence of dichlorofluorescein were calculated by the value of maximal fluorescence intensity (*F*) during 20 min of stimulation and initial value of fluorescence, F_0. *, $p < 0.05$; **, $p < 0.01$ *versus* PTX-untreated or LacZ-expressing cells. *Error bars*, S.E.

PX, a specific marker for PI-3-P, was expressed (53). Under the basal condition, $p40^{phox}$-PX was predominantly localized in the PI-3-P-enriched early endosome and nucleus (Fig. 4*D*). Treatment with PTX for 10 min promoted the translocation of $p40^{phox}$-PX from early endosome to the plasma membrane. However, PTX did not affect the localization of $p40^{phox}$-PX (R105K), a mutant that cannot recognize PI-3-P. The localization of the PH domain of GRP1 (54), a marker for PI 3,4,5-trisphosphate, and that of the PH domain of PLCδ1, a marker for PI 4,5-bisphosphate, were not changed by PTX (data not shown). These results suggest that PTX-induced PI-3-P production through PI 3-kinase activation is required for translocation and activation of Rac.

Involvement of Rac in PTX-induced ROS Production—One of the targets for Rac is NADPH oxidase. Because the PTX-induced NF-κB activation was suppressed by DPI, DN-Rac, and DN-$p47^{phox}$ (Fig. 3*F*), Rac-mediated activation of NADPH oxidase may participate in PTX-induced NF-κB activation. We found that PTX gradually increased dichlorofluorescein fluorescence intensity, indicating ROS production in cardiac fibroblasts (Fig. 5). The expression of DN-Rac completely sup-

pressed this ROS production, suggesting that PTX activates Rac and turns on a signaling cascade downstream of Rac.

Essential Role of Rac in PTX-induced AT1R Up-regulation—Because PTX-induced ROS production, NF-κB activation, and increase in AT1R density were inhibited by DN-Rac, Rac may play a central role in regulation of AT1R density. Inhibitors of 3-hydroxy-3-methylglutaryl-CoA reductase (statins) are known to suppress the activity of Rho family G proteins by inhibition of isoprenylation (55). It has been reported that simvastatin inhibits Rac activity in the H9c2 cell line and rat neonatal cardiomyocytes (56, 57). Simvastatin is also reported to reduce AT1R density in vascular smooth muscle cells (58). Therefore, we examined whether simvastatin inhibits IL-1β-induced up-regulation of AT1R by inhibition of Rac. Treatment with simvastatin completely suppressed the IL-1β-induced Rac activation (supplemental Fig. 4). Consistent with this result, the IL-1β-induced up-regulation of AT1R was also suppressed by simvastatin and DN-Rac. The Ang II-induced Ca^{2+} release was also enhanced in IL-1β-treated cells, and this enhancement was completely suppressed by simvastatin. These results suggest that simvastatin suppresses IL-1β-induced up-regulation of AT1R by inhibition of Rac activity. To prove the requirement of Rac in AT1R up-regulation more directly, we used Rac1 siRNAs. Knockdown of Rac1 almost completely suppressed IL-1β-induced Rac activation (Fig. 6*A*), increase in AT1R density (Fig. 6*B*), and enhancement of AT1R-stimulated Ca^{2+} responses (supplemental Fig. 4). Thus, Rac1 may predominantly regulate AT1R up-regulation by agonist stimulation. Because IL-1β induces Rac activation and PTX-induced IL-1β production was completely suppressed by knockdown of Rac1 (Fig. 6*C*), we hypothesize that PTX-induced IL-1β production plays a role in amplification of Rac activation. Treatment with IL-1β siRNA suppressed the PTX-induced Rac activation at a late phase of activation (from 6 h after the treatment) but did not suppress Rac activation at an early phase of activation (Fig. 6, *D* and *E*). Furthermore, IL-1β siRNA also suppressed PTX-induced nuclear localization of NF-κB in a late phase but not an early phase (Fig. 6, *F* and *G*). These results suggest that PTX-induced IL-1β production participates in the sustained activation of Rac and NF-κB, which is essential for AT1R up-regulation.

PTX Stimulates TLR4, Leading to Rac Activation—We next examined which receptor(s) functions as a target of PTX in cardiac fibroblasts. Because TLR4 is reported to work as a putative candidate receptor of B-oligomer (10), we examined whether stimulation of TLR4 is required for PTX-induced AT1R up-regulation in cardiac fibroblasts. Treatment with TLR4 siRNAs (si-88, si-1002, and si-1621) significantly decreased TLR4 mRNA levels but did not decrease AT1R mRNA levels (Fig. 7*A*). The PTX-induced enhancement of Ang II-induced Ca^{2+} release and increase in Rac activity were completely abolished by TLR4 siRNA treatment (Fig. 7, *B* and *C*). In contrast, PTX-induced ADP-ribosylation of $G\alpha_i$ proteins was not suppressed but preferably enhanced by TLR4 knockdown (Fig. 7*D*). These results suggest that TLR4 mediates PTX-induced Rac activation and AT1R up-regulation, but TLR4 does not mediate PTX-induced ADP-ribosylation of $G\alpha_i$ proteins.

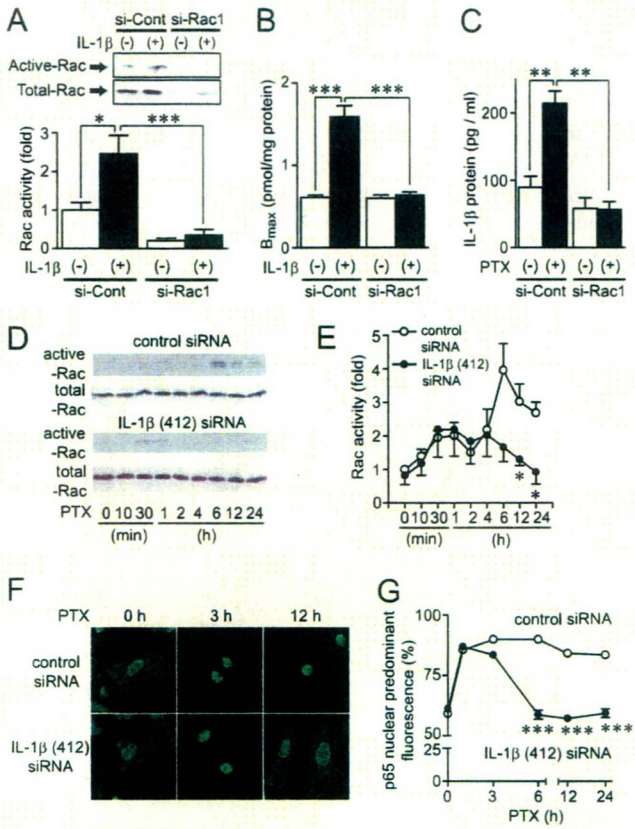

FIGURE 6. **Amplification of Rac-mediated signaling by PTX-induced IL-1β production.** *A*, cells were transfected with siRNAs for Rac1 (*si-Rac1*) or their randomized controls (*si-Cont*) for 72 h before 5-min stimulation with IL-1β (10 ng/ml). *B*, effects of si-Rac1 on the maximal increases in AT1R density by IL-1β stimulation. Cells were treated with IL-1β for 24 h before membrane preparation. *C*, effects of si-Rac1 on PTX-induced production of IL-1β proteins. Cells were treated with PTX (100 ng/ml) for 90 min. *D* and *E*, effects of IL-1β siRNA on PTX-induced Rac activation. Cells were transfected with IL-1β (412) siRNA (100 nM) for 48 h before treatment with PTX (100 ng/ml). *F* and *G*, effects of IL-1β (412) siRNA on PTX-induced nuclear localization of the NF-κB p65 subunit. More than 100 cells were scanned and quantified the subcellular localization of p65 using Photoshop (13, 27). *, $p < 0.05$; ***, $p < 0.001$ *versus* IL-1β-treated or control siRNA-treated cells. *Error bars*, S.E.

DISCUSSION

In this study, we demonstrated a novel action of PTX that enhances AT1R-stimulated Ca^{2+} response through AT1R up-regulation independently of ADP-ribosylation in rat cardiac fibroblasts. Using PTX as a powerful tool for analyzing the mechanism of AT1R up-regulation, we demonstrated that stimulation of TLR4 by PTX B-oligomer enhances AT1R function. Previous reports have suggested that Syk (spleen tyrosine kinase) and PI 3-kinase participate in TLR4-mediated responses (49, 59). We found that PTX-induced Rac activation was completely suppressed by inhibition of Syk (supplemental Fig. 3) and PI 3-kinase (Fig. 5), suggesting that Syk and PI 3-kinase mediate PTX-induced Rac activation. We also found that Rac-mediated NF-κB activation through ROS production plays a central role in the regulation of AT1R density. The PTX-induced NF-κB activation was suppressed by DPI and the dominant negative mutants of Rac and $p47^{phox}$ (Fig. 3). Because DPI is an inhibitor of NADPH oxidase and Rac and $p47^{phox}$ are essential compo-

nents of NADPH oxidase activation, the origin of PTX-induced ROS production may be NADPH oxidase. In addition, PTX induced degradation of IκBα proteins in a time-dependent manner, which was abolished by Rac inhibition (supplemental Fig. 3). Although molecular mechanism underlying ROS-mediated NF-κB activation is still unknown, this result implies that ROS-mediated inhibition of mitogen-activated protein kinase phosphatases may be involved (60). Because the promoter regions of IL-1β and AT1R contain a putative NF-κB binding site, AT1R up-regulation may be induced by direct interaction of AT1R promoter with NF-κB. However, PTX-induced enhancement of Ca^{2+} response by AT1R stimulation was almost completely suppressed by anti-IL-1β antibody and IL-1β siRNAs (Fig. 2). Thus, IL-1β released from fibroblasts by PTX treatment may be the main mechanism of PTX-induced AT1R up-regulation. Furthermore, Rac1 inhibition suppressed PTX-induced IL-1β production, and IL-1β inhibition suppressed PTX-induced Rac activation at a late but not an early phase (Fig. 6). Thus, Rac-mediated IL-1β production may amplify Rac-dependent signaling through IL-1β-mediated Rac activation. These results suggest that PTX induces AT1R up-regulation through a TLR4 → PI 3-kinase → Rac → NADPH oxidase → ROS → NF-κB → IL-1β-dependent signal pathway (Fig. 8).

We revealed that stimulation of TLR4 mediates PTX-induced AT1R up-regulation. It is thought that MyD88 and Trif-related adaptor molecule mediate TLR4-mediated NF-κB activation (32). However, it has recently been reported that oxidized LDL induces NADPH oxidase-dependent ROS production through TLR4 stimulation in macrophages (59). These authors have also demonstrated that Syk but not MyD88 is responsible for TLR4-mediated ROS production. In addition, another study has shown that stimulation of TLR4 by PTX B-oligomer induces activation of MyD88-independent signaling pathways (10). Thus, PTX induces stimulation of TLR4 that preferentially activates the Syk-dependent Rac signaling pathway.

PTX is frequently used as a specific tool to examine the involvement of G_i in cellular signaling. Abolishment of TLR4 by siRNA did not affect PTX-mediated ADP-ribosylation of G_i and G_o (Fig. 7*D*). Thus, PTX binds to two receptors; one is TLR4 that activates Rac and another is the binding site that liberates the A-protomer into cells. So far, the G_i/G_o-independent signaling pathway is not usually considered when PTX is used *in vitro* and *in vivo*. Because PTX activates Rac in addition to ADP-ribosylation of G_i and G_o, it is no longer thought that PTX is a specific inhibitor of receptor-G_i signaling.

Another important finding of this study is that Rac is a physiological mediator of AT1R up-regulation induced by IL-1β stimulation. The inhibition of Rac suppressed the increase in AT1R density and the enhancement of Ang II-induced Ca^{2+} response by IL-1β stimulation (Fig. 6 and supplemental Fig. 4). Because other agonists that up-regulate AT1R, such as Ang II and TNF-α, also increase Rac activity, Rac-mediated AT1R up-regulation may be a common mechanism among various stimuli. Statins are inhibitors of 3-hydroxy-3-methylglutaryl-CoA reductase and appear

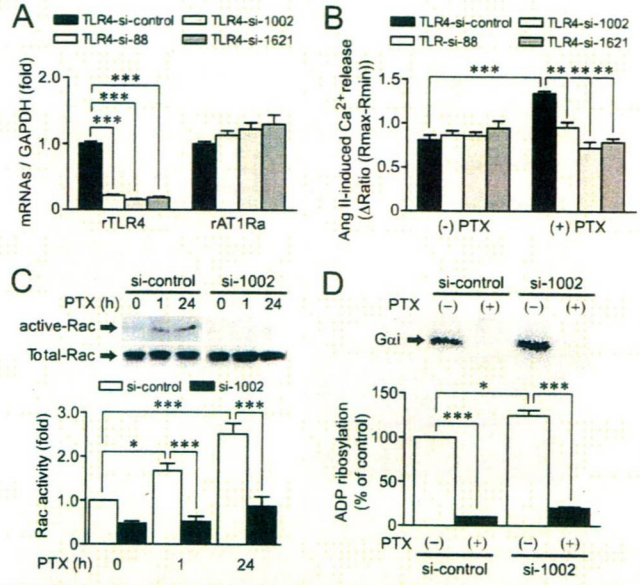

FIGURE 7. **Roles of TLR4 in PTX-induced Rac activation and ADP-ribosylation of G_i/G_o.** *A*, effects of TLR4 siRNAs on the expression of TLR4 and AT1R mRNAs. *B*, effects of TLR4 siRNAs on PTX-induced enhancement of Ang II-induced Ca^{2+} responses. Cells were treated with PTX for 24 h after siRNA treatment for 48 h. *C*, effects of TLR4 siRNA (si-1002) on PTX-induced Rac activation. *D*, effects of TLR4 siRNA on PTX-induced ADP-ribosylation of $G\alpha_i$ proteins. *, $p < 0.05$; **, $p < 0.01$; ***, $p < 0.001$. *Error bars*, S.E.

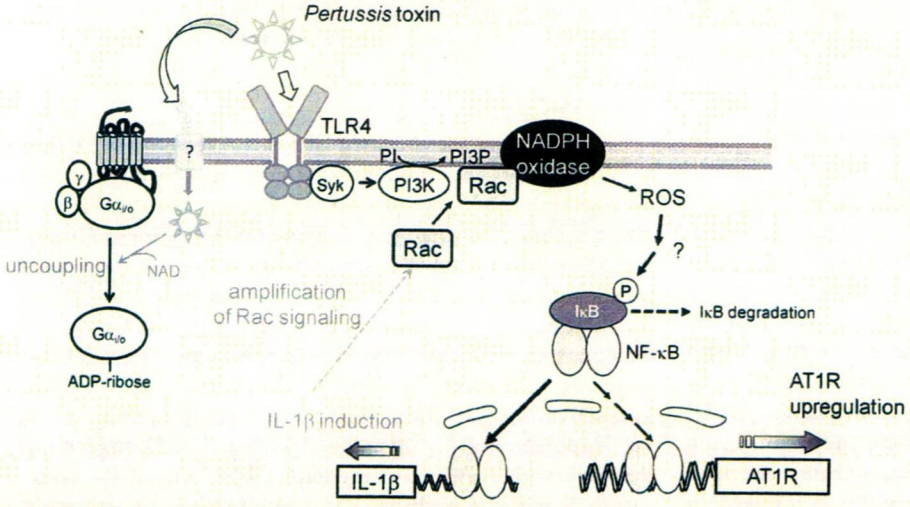

FIGURE 8. **Schema of TLR4-mediated AT1R up-regulation induced by PTX.** PTX induces ROS production through sequential activation of TLR4, Syk, PI 3-kinase (*PI3K*), Rac, and NADPH oxidase. Although the mechanism of NF-κB activation induced by ROS is still unknown, ROS mediate NF-κB-dependent expression of IL-1β. Induction of IL-1β also induces Rac activation through IL-1 receptor stimulation, leading to amplification of Rac-dependent signaling. Sustained activation of Rac may be required for PTX-induced AT1R up-regulation in rat cardiac fibroblasts. A-protomer of PTX enters the cells through unidentified binding site, and ADP-ribosylates G_i/G_o proteins.

to have pleiotropic effects on the cardiovascular system that are independent of their ability to decrease serum cholesterol (14, 55). These include inhibition of cardiac hypertrophy and left ventricular dysfunction, anti-inflammatory effects, and antioxidative effects (55, 61). Recent studies have demonstrated that statins inhibit ROS production and myocardial apoptosis by inhibition of Rac (57). Up-regulation of AT1R is thought to be one of the features involved in cardiac remodeling. Thus, the present results suggest a novel mechanism in which statins inhibit cardiac fibrosis by inhibition of AT1R up-regulation in cardiac fibroblasts. Statins also inhibit Rho activity by inhibition of isoprenylation. However, we could not detect the activation of Rho, Ras, and Rap1 by PTX treatment (supplemental Fig. 2). Thus, inhibition of Rac is essential for the inhibition of AT1R up-regulation by statin.

In conclusion, we demonstrated a novel action of PTX that induces AT1R up-regulation independently of ADP-ribosylation of G_i/G_o. This mechanism includes TLR4-mediated Rac activation, ROS production, and NF-κB activation. Activation of NF-κB induces IL-1β production, resulting in amplification of Rac signaling, which leads to increase in AT1R density. The involvement of the TLR4-Rac signaling pathway in the regulation of AT1R density will provide a possible novel target for inhibiting cardiac remodeling. In addition, we have provided pharmacologically important information indicating that PTX *per se* influences G protein-coupled receptor signaling independently of $G\alpha_i$ inhibition. Activation of the TLR4-Rac signaling pathway by PTX suggests that we should consider pharmacological actions of PTX in addition to a specific inhibitor of G_i/G_o-mediated signal transduction.

Acknowledgment—We thank Miyuki Toyotaka for analyzing the localization of the NF-κB p65 subunit.

REFERENCES

1. Katada, T., and Ui, M. (1982) *J. Biol. Chem.* **257,** 7210–7216
2. Kurose, H., Katada, T., Amano, T., and Ui, M. (1983) *J. Biol. Chem.* **258,** 4870–4875
3. Tamura, M., Nogimori, K., Yajima, M., Ase, K., and Ui, M. (1983) *J. Biol. Chem.* **258,** 6756–6761
4. Lando, Z., Teitelbaum, D., and Arnon, R. (1980) *Nature* **287,** 551–552
5. Linthicum, D. S., Munoz, J. J., and Blaskett, A. (1982) *Cell Immunol.* **73,** 299–310
6. Racke, M. K., Hu, W., and Lovett-Racke, A. E. (2005) *Trends Immunol.* **26,** 289–291
7. Jajoo, S., Mukherjea, D., Pingle, S., Sekino, Y., and Ramkumar, V. (2006) *J. Pharmacol. Exp. Ther.* **317,** 1–10
8. Li, H., and Wong, W. S. (2001) *Biochem. Biophys. Res. Commun.* **283,** 1077–1082
9. Melien, O., Sandnes, D., Johansen, E. J., and Christoffersen, T. (2000) *J. Cell Physiol.* **184,** 27–36
10. Wang, Z. Y., Yang, D., Chen, Q., Leifer, C. A., Segal, D. M., Su, S. B., Caspi, R. R., Howard, Z. O., and Oppenheim, J. J. (2006) *Exp. Hematol.* **34,** 1115–1124
11. Timmermans, P. B., Wong, P. C., Chiu, A. T., Herblin, W. F., Benfield, P., Carini, D. J., Lee, R. J., Wexler, R. R., Saye, J. A., and Smith, R. D. (1993) *Pharmacol. Rev.* **45,** 205–251
12. de Gasparo, M., Catt, K. J., Inagami, T., Wright, J. W., and Unger, T. (2000) *Pharmacol. Rev.* **52,** 415–472
13. Onohara, N., Nishida, M., Inoue, R., Kobayashi, H., Sumimoto, H., Sato, Y., Mori, Y., Nagao, T., and Kurose, H. (2006) *EMBO J.* **25,** 5305–5316
14. Brown, R. D., Ambler, S. K., Mitchell, M. D., and Long, C. S. (2005) *Annu. Rev. Pharmacol. Toxicol.* **45,** 657–687
15. Villarreal, F. J., Kim, N. N., Ungab, G. D., Printz, M. P., and Dillmann, W. H. (1993) *Circulation* **88,** 2849–2861
16. Sakata, Y., Hoit, B. D., Liggett, S. B., Walsh, R. A., and Dorn, G. W., 2nd (1998) *Circulation* **97,** 1488–1495
17. Gurantz, D., Cowling, R. T., Varki, N., Frikovsky, E., Moore, C. D., and Greenberg, B. H. (2005) *J. Mol. Cell Cardiol.* **38,** 505–515
18. Nio, Y., Matsubara, H., Murasawa, S., Kanasaki, M., and Inada, M. (1995) *J. Clin. Invest.* **95,** 46–54
19. Yamani, M. H., Cook, D. J., Tuzcu, E. M., Abdo, A., Paul, P., Ratliff, N. B., Yu, Y., Yousufuddin, M., Feng, J., Hobbs, R., Rincon, G., Bott-Silverman, C., McCarthy, P. M., Young, J. B., and Starling, R. C. (2004) *Am. J. Transplant.* **4,** 1097–1102
20. Peng, J., Gurantz, D., Tran, V., Cowling, R. T., and Greenberg, B. H. (2002) *Circ. Res.* **91,** 1119–1126
21. Finkel, T. (1999) *J. Leukoc. Biol.* **65,** 337–340
22. Griendling, K. K., and Ushio-Fukai, M. (2000) *Regul. Pept.* **91,** 21–27
23. Sundaresan, M., Yu, Z. X., Ferrans, V. J., Sulciner, D. J., Gutkind, J. S., Irani, K., Goldschmidt-Clermont, P. J., and Finkel, T. (1996) *Biochem. J.* **318,** 379–382
24. Sumimoto, H. (2008) *FEBS J.* **275,** 3249–3277
25. Sulciner, D. J., Irani, K., Yu, Z. X., Ferrans, V. J., Goldschmidt-Clermont, P., and Finkel, T. (1996) *Mol. Cell Biol.* **16,** 7115–7121
26. Nishida, M., Tanabe, S., Maruyama, Y., Mangmool, S., Urayama, K., Nagamatsu, Y., Takagahara, S., Turner, J. H., Kozasa, T., Kobayashi, H., Sato, Y., Kawanishi, T., Inoue, R., Nagao, T., and Kurose, H. (2005) *J. Biol. Chem.* **280,** 18434–18441
27. Fujii, T., Onohara, N., Maruyama, Y., Tanabe, S., Kobayashi, H., Fukutomi, M., Nagamatsu, Y., Nishihara, N., Inoue, R., Sumimoto, H., Shibasaki, F., Nagao, T., Nishida, M., and Kurose, H. (2005) *J. Biol. Chem.* **280,** 23041–23047
28. Pracyk, J. B., Tanaka, K., Hegland, D. D., Kim, K. S., Sethi, R., Rovira, I. I., Blazina, D. R., Lee, L., Bruder, J. T., Kovesdi, I., Goldshmidt-Clermont, P. J., Irani, K., and Finkel, T. (1998) *J. Clin. Invest.* **102,** 929–937
29. Sussman, M. A., Welch, S., Walker, A., Klevitsky, R., Hewett, T. E., Price, R. L., Schaefer, E., and Yager, K. (2000) *J. Clin. Invest.* **105,** 875–886
30. Ichiki, T., Takeda, K., Tokunou, T., Iino, N., Egashira, K., Shimokawa, H., Hirano, K., Kanaide, H., and Takeshita, A. (2001) *Arterioscler. Thromb. Vasc. Biol.* **21,** 1896–1901
31. Akira, S., Uematsu, S., and Takeuchi, O. (2006) *Cell* **124,** 783–801
32. Chao, W. (2009) *Am. J. Physiol. Heart Circ. Physiol.* **296,** H1–H12
33. Kurose, H., Arriza, J. L., and Lefkowitz, R. J. (1993) *Mol. Pharmacol.* **43,** 444–450
34. Nishida, M., Sato, Y., Uemura, A., Narita, Y., Tozaki-Saitoh, H., Nakaya, M., Ide, T., Suzuki, K., Inoue, K., Nagao, T., and Kurose, H. (2008) *EMBO J.* **27,** 3104–3115
35. Nishida, M., Sugimoto, K., Hara, Y., Mori, E., Morii, T., Kurosaki, T., and Mori, Y. (2003) *EMBO J.* **22,** 4677–4688
36. Nagamatsu, Y., Nishida, M., Onohara, N., Fukutomi, M., Maruyama, Y., Kobayashi, H., Sato, Y., and Kurose, H. (2006) *J. Pharmacol. Sci.* **101,** 144–150
37. Chiloeches, A., Paterson, H. F., Marais, R., Clerk, A., Marshall, C. J., and Sugden, P. H. (1999) *J. Biol. Chem.* **274,** 19762–19770
38. Franke, B., Akkerman, J. W., and Bos, J. L. (1997) *EMBO J.* **16,** 252–259
39. Arai, K., Maruyama, Y., Nishida, M., Tanabe, S., Takagahara, S., Kozasa, T., Mori, Y., Nagao, T., and Kurose, H. (2003) *Mol. Pharmacol.* **63,** 478–488
40. Ju, H., Zhao, S., Tappia, P. S., Panagia, V., and Dixon, I. M. (1998) *Circulation* **97,** 892–899
41. Bai, H., Wu, L. L., Xing, D. Q., Liu, J., and Zhao, Y. L. (2004) *Chin. Med. J.* **117,** 88–93
42. He, J., Gurunathan, S., Iwasaki, A., Ash-Shaheed, B., and Kelsall, B. L. (2000) *J. Exp. Med.* **191,** 1605–1610
43. Maruyama, Y., Nishida, M., Sugimoto, Y., Tanabe, S., Turner, J. H., Kozasa, T., Wada, T., Nagao, T., and Kurose, H. (2002) *Circ. Res.* **91,** 961–969
44. Nishida, M., Maruyama, Y., Tanaka, R., Kontani, K., Nagao, T., and Kurose, H. (2000) *Nature* **408,** 492–495

45. Cowling, R. T., Gurantz, D., Peng, J., Dillmann, W. H., and Greenberg, B. H. (2002) *J. Biol. Chem.* **277,** 5719–5724
46. Monks, B. G., Martell, B. A., Buras, J. A., and Fenton, M. J. (1994) *Mol. Immunol.* **31,** 139–151
47. Kaiser, P., Rothwell, L., Goodchild, M., and Bumstead, N. (2004) *Anim. Genet.* **35,** 169–175
48. Cowling, R. T., Zhang, X., Reese, V. C., Iwata, M., Gurantz, D., Dillmann, W. H., and Greenberg, B. H. (2005) *Am. J. Physiol. Heart Circ. Physiol.* **289,** H1176–H1183
49. Zocchi, M. R., Contini, P., Alfano, M., and Poggi, A. (2005) *J. Immunol.* **174,** 6054–6061
50. Ueyama, T., Eto, M., Kami, K., Tatsuno, T., Kobayashi, T., Shirai, Y., Lennartz, M. R., Takeya, R., Sumimoto, H., and Saito, N. (2005) *J. Immunol.* **175,** 2381–2390
51. van Hennik, P. B., ten Klooster, J. P., Halstead, J. R., Voermans, C., Anthony, E. C., Divecha, N., and Hordijk, P. L. (2003) *J. Biol. Chem.* **278,** 39166–39175
52. Brown, G. E., Stewart, M. Q., Liu, H., Ha, V. L., and Yaffe, M. B. (2003) *Mol. Cell* **11,** 35–47
53. Honbou, K., Minakami, R., Yuzawa, S., Takeya, R., Suzuki, N. N., Kamakura, S., Sumimoto, H., and Inagaki, F. (2007) *EMBO J.* **26,** 1176–1186
54. Gray, A., Van Der Kaay, J., and Downes, C. P. (1999) *Biochem. J.* **344,** 929–936
55. Rikitake, Y., and Liao, J. K. (2005) *Circ. Res.* **97,** 1232–1235
56. Ichiki, T., Takeda, K., Tokunou, T., Funakoshi, Y., Ito, K., Iino, N., and Takeshita, A. (2001) *Hypertension* **37,** 535–540
57. Laufs, U., Kilter, H., Konkol, C., Wassmann, S., Böhm, M., and Nickenig, G. (2002) *Cardiovasc. Res.* **53,** 911–920
58. Ito, M., Adachi, T., Pimentel, D. R., Ido, Y., and Colucci, W. S. (2004) *Circulation* **110,** 412–418
59. Bae, Y. S., Lee, J. H., Choi, S. H., Kim, S., Almazan, F., Witztum, J. L., and Miller, Y. I. (2009) *Circ. Res.* **104,** 210–218
60. Kamata, H., Honda, S., Maeda, S., Chang, L., Hirata, H., and Karin, M. (2005) *Cell* **120,** 649–661
61. Maack, C., Kartes, T., Kilter, H., Schäfers, H. J., Nickenig, G., Böhm, M., and Laufs, U. (2003) *Circulation* **108,** 1567–1574

European Journal of Pharmacology 635 (2010) 56–61

Contents lists available at ScienceDirect

European Journal of Pharmacology

journal homepage: www.elsevier.com/locate/ejphar

Neuropharmacology and Analgesia

Protective effect of all-trans retinoic acid on NMDA-induced neuronal cell death in rat retina

Kenji Sakamoto [a,*], Masahide Hiraiwa [a], Maki Saito [a], Tsutomu Nakahara [a], Yoji Sato [b], Taku Nagao [c], Kunio Ishii [a]

[a] Department of Molecular Pharmacology, Kitasato University School of Pharmaceutical Sciences, 9-1 Shirokane 5-chome, Minato-ku, Tokyo 108-8641, Japan
[b] Division of Cellular and Gene Therapy Products, National Institute of Health Sciences, 18-1 Kamiyoga 1-chome, Setagaya-ku, Tokyo 158-8501, Japan
[c] National Institute of Health Sciences, 18-1 Kamiyoga 1-chome, Setagaya-ku, Tokyo 158-8501, Japan

ARTICLE INFO

Article history:
Received 17 August 2009
Received in revised form 30 January 2010
Accepted 3 March 2010
Available online 19 March 2010

Keyword:
All-trans retinoic acid
Retina
N-methyl-D-aspartic acid
Extracellular signal-regulated kinase

ABSTRACT

We histologically examined the effects of all-trans retinoic acid (ATRA) on neuronal injury induced by intravitreous injection of N-methyl-D-aspartic acid (NMDA) (200 nmol/eye). Treatment with ATRA for 7 days (15 mg/kg for the first two days and 10 mg/kg for the following five days, p.o.) reduced the decrease of cell number in the ganglion cell layer and the inner nuclear layer 7 days after NMDA injection. TUNEL staining 6 h after NMDA injection showed that treatment with ATRA (15 mg/kg, p.o.) 1 h prior to NMDA injection reduced the number of apoptotic cells in the ganglion cell layer and inner nuclear layer. The anti-apoptotic effect of ATRA was vanished by intravitreous injection of U0126, an extracellular signal-regulated kinase/mitogen-activated protein kinase kinase inhibitor (1 nmol/eye). These results suggest that ATRA has a protective effect, which is medicated by extracellular signal-regulated kinase pathway, on NMDA-induced apoptosis in the rat retina. ATRA may be useful as a therapeutic drug against retinal diseases that cause glutamate neurotoxicity.

1. Introduction

Cell death of retinal ganglion cells is a characteristic of glaucoma, and the underlying mechanism is not completely understood. Stimulation of glutamate receptors by excess amount of glutamate under hypoxia (David et al., 1988) and ischemia–reperfusion (Louzada-Júnior et al., 1992) is toxic to neuronal cells. Activation of the N-methyl-D-aspartic acid (NMDA) receptor, a subtype of glutamate receptors (Choi, 1987, 1988), followed by excess Ca^{2+} influx *via* NMDA receptor-operated channels is involved in the predominant mechanism of neuronal excitotoxicity. In fact, excitotoxicity caused by the elevation of glutamate concentration in the retinal extracellular space near the glutamate receptors is thought to be one of the mechanisms of neuronal cell death induced by glaucoma (Kuehn et al., 2005).

Retinoids, including vitamin A and its derivatives, play important roles for regulating various biological processes, such as visual function, growth and differentiation (Chambon, 1996; Maden, 2001). Retinal and opsin comprise rhodopsin, which is very important for normal visual function (Palczewski et al., 2000). Retinoic acids regulate the expression of various genes by activation of their nuclear receptors, retinoic acid receptors and retinoid X receptors (Chambon, 1996; Maden, 2001). Retinoic acids bound to these receptors are transported to nucleus and work as transcription factors (Chambon, 1994). Recently, retinoic acids were reported to have rapid non-genomic effects on cytoplasmic messenger pathways. For example, retinoic acids have been reported to cause a rapid activation of extracellular signal-regulated kinase (ERK) through retinoic acid receptors and/or retinoid X receptors (Canon et al., 2004; Pasquali et al., 2005).

Retinoic acids are reported to play significant roles under pathological conditions. For instance, all-trans retinoic acid (ATRA) has a protective effect on oxygen–glucose deprivation-medicated cell death in the rat hippocampus slice *via* inhibition of c-jun N-terminal kinase and p38 mitogen-activated protein kinase (Shinozaki et al., 2007). Although retinoic acids have very important roles in the visual signal transduction, the role of the signaling cascade of retinoic acid in pathological conditions such as glaucoma in the retina still remains uncertain.

Mitogen-activated protein (MAP) kinase family plays important roles in the transduction of various extracellular stimuli to the nucleus. The family consists of three subgroups, extracellular signal-regulated kinase (ERK), c-jun N-terminal kinase (JNK) and p38 MAP kinase. Recent studies show that ATRA prevents neuronal cell death induced by beta-amyloid (Sahin et al., 2005), staurosporine (Ahlemeyer and Krieglstein, 1998), and oxygen–glucose deprivation (Shinozaki et al., 2007), and rapidly activated ERK *via* retinoic acid receptor in neuronal cells (Canon et al., 2004). Brain-derived neurotrophic factor and erythropoietin have been shown to protect against neuronal cell death induced by glutamate, hypoxia or ischemia *via* activation of ERK (Hetman et al., 1999; Han and Holtzman, 2000; Rössler et al., 2004; Kilic et al., 2005).

* Corresponding author. Tel./fax: +81 3 3444 6205.
E-mail address: sakamotok@pharm.kitasato-u.ac.jp (K. Sakamoto).

0014-2999/$ – see front matter © 2010 Elsevier B.V. All rights reserved.
doi:10.1016/j.ejphar.2010.03.001

Based on these finding shown above, we hypothesized that activation of retinoid acid signaling would protect against NMDA-induced neuronal cell death in the retina. In the present study, we demonstrated that ATRA protected the retinal neuron against apoptosis induced by NMDA. Because much better tolerance of retinoic acid was shown when using single doses (Teelmann, 1989), a single dose per day was chosen instead of multiple doses. The doses of ATRA used in this study were chosen according to doses tested in previous studies by other researchers. The dose of ATRA (15 mg/kg for the first two days and 10 mg/kg for the following five days, p.o.) has been shown to have anti-inflammatory properties in experimental rat models of nephropathy (Moreno-Manzano et al., 2003), to enhance nociceptive withdrawal reflexes in rats (Romero-Sandoval et al., 2004), and also to induce an increase in the prostaglandin E2 concentration in rat plasma and liver homogenate (Devaux et al., 2001). They were also well below the toxic doses reported in similar species (Teelmann, 1989). To test whether the protective effects of ATRA is dose-dependent, we tried one-third dose and three-time dose of ATRA. We also showed that the anti-apoptotic effect of ATRA was reduced by U0126, an extracellular signal-regulated kinase/mitogen-activated protein kinase kinase (MEK) inhibitor.

2. Materials and methods

2.1. Animals

In the present study, experimental procedures conformed to the Guiding Principles for the Care and Use of Laboratory Animals, approved by the Japanese Pharmacological Society. Male Sprague–Dawley rats weighing 230–300 g (Charles River Japan, Kanagawa, Japan) were used in the present study.

2.2. Intravitreous injection

Intravitreous injection was performed as previously described (Siliprandi et al., 1992; Sakamoto et al., 2009). Briefly, rats were anesthetized by intraperitoneal injection of sodium pentobarbital (50 mg/kg i.p.; Nembutal® injection, Abbott Laboratories, North Chicago, IL). Injection was performed with a 33-gauge needle connected to a 25-μl gas-tight microsyringe (1702LT, Hamilton, Reno, NV). The tip of the needle was inserted approximately 1 mm behind the corneal limbus. Five μl of the drug solution described below was administered into one eye and vehicle was administered into another eye as control.

2.3. Preparation of drugs

NMDA (Nacalai Tesque, Kyoto, Japan) were dissolved in saline. All-trans retinoic acid (ATRA) (Sigma, St. Louis, MO) was suspended in 0.5% carboxymethyl cellulose (CMC) (Nacalai Tesque), and orally administered. The final volume of the suspension is 0.5 ml. A similar amount of 0.5% CMC was administered to the control animals. In the continuous administration with either ATRA or vehicle for seven days, the dose of ATRA in the first two days was 5, 15 or 45 mg/kg and the dose in the following five days was 3, 10 or 30 mg/kg, respectively. In the single administration of ATRA, 15 mg/kg ATRA was treated. The first dose of ATRA or the vehicle was administered orally 1 h before NMDA injection. We prepared 0.4 M stock solutions of U0126 (Promega, Madison, WI) and diluted it to working concentration (2×10^{-4} M or 4×10^{-4} M) with saline. U0126 or the vehicle was administrated intravitreously 15 min before treatment of ATRA.

2.4. Histological evaluation

The method for histological evaluation was described previously (Sakamoto et al., 2006; Sakamoto et al., 2009). The method is a modification of the one employed by some other groups (LaVail and Battelle, 1975; Unoki and LaVail, 1994; Roth et al., 1998; Toriu et al., 2000). Animals were euthanized by overdosage of pentobarbital sodium 7 days after intravitreous NMDA injection and both eyes were enucleated. Enucleated eyes were fixed with Davidson solution, comprised of 37.5% ethanol, 9.3% paraformaldehyde, 12.5% acetic acid and 3% glutaraldehyde for 1–12 h at room temperature. The fixed eye was bisected through the optic nerve head in the vertical meridian with a microtome blade (Histo Cutter Super #35 Type, Micro Glass, Tokyo, Japan) and embedded in paraffin after removing a lens. Five μm horizontal sections through the optic nerve head of the eye were cut along the vertical meridian of the eye so as to contain the entire retina from the ora serrata in the superior hemisphere to the ora serrata in the inferior hemisphere using a microtome (HM325, Microm International, Walldorf, Germany) and a microtome blade (Histo Cutter Super #35 Type, Micro Glass). The sections were stained with hematoxylin and eosin, and subject to morphometry. The sections which showed oblique regions were excluded to avoid artifacts. The total number of the cells in the retinal ganglion cell layer (GCL) was counted for a length of 1 mm on either side of the optic nerve head beginning approximately 1 mm from the center of the optic nerve head in four independent sections using a light microscope (Optiphot-2, Nicon, Tokyo, Japan). No attempt was made to distinguish the cell types in the GCL, and displaced amacrine cells were not excluded from the counts. Measurement of the thickness of the inner plexiform layer (IPL), the inner nuclear layer (INL) and the outer nuclear layer (ONL) was also performed to quantify the degree of cell loss induced by intravitreous NMDA injection. Digital photographs with approximately 0.25 mm width of the retinal layers in each section at a distance of approximately 1 mm from the center of the optic nerve head were taken using a digital camera (DP11, Olympus, Tokyo, Japan) connected to a light microscope. The photographs were printed onto A4 papers. Lines indicating the inner and outer borders of INL and ONL and the bottom of the ganglion cells were drawn on the printed photographs. To know the thicknesses of IPL, INL and ONL, the distance between the lines on the paper was measured. The areas which measured the distance were spaced at approximately 40 μm intervals. Averages for these measurements of thickness taken in five adjacent areas were calculated. These parameters of each eye injected NMDA were normalized with those of the corresponding intact opposite eyes and are presented as percentages. We did all of the morphometrical analysis in a blind fashion.

2.5. Deoxy UTP-biotin nick-end labeling assay

The method for terminal deoxynucleotidyl transferase-mediated dUTP-biotin nick-end labeling (TUNEL) assay was described previously (Sakamoto et al., 2009). To examine whether ATRA inhibits apoptosis induced by intravitreous NMDA injection, TUNEL assay was performed. Intravitreous NMDA injection was performed as described above in one eye and saline was injected to another eye as control. Animals were euthanized by overdosage of pentobarbital sodium 6 h after NMDA injection and both eyes were enucleated. Enucleated eyes were fixed with Davidson solution described above for 1 h at room temperature. Fixed retinal tissues were cryoprotected in Holt's hypertonic gum sucrose solution, comprised of 0.1% thymol, 1% gum acacia and 30% sucrose in distilled water, overnight at 4 °C. Ten-μm-thick sections of retina through the optic disk were then cut with a cryostat (HM 500, Microm International, Walldorf, Germany). The TUNEL assay was performed with ApoTag peroxidase in situ apoptosis detection kit (Chemicon, Temecula, CA), according to the manufacturer's instructions. For nuclear staining, the specimens were counterstained with methylgreen (Wako Pure Chemical, Osaka, Japan). We counted the number of TUNEL-positive nuclei in GCL and INL for a length of 1 mm on either side of the optic nerve head

beginning approximately 1 mm from the center of the optic nerve head manually using a light microscope.

2.6. Statistical analysis

The data represent the means ± S.E.M. of three to ten rats per group. One way analysis of variance followed by Tukey–Kramer test was used for multiple comparisons. Differences were considered to be statistically significant when the P values were less than 0.05.

3. Results

3.1. Effect of ATRA on the retinal injury induced by the intravitreous NMDA injection

At first, we determined the effects of ATRA on the retinal injury induced by intravitreous NMDA injection. Typical photomicrographs of the retina taken 7 days after NMDA injection are shown in Fig. 1. In the vehicle-treated group, degenerative changes were observed in GCL and IPL of the NMDA-injected eye, a characteristic of retinal atrophy (Fig. 1B), but such changes were not seen in the contralateral control retina (Fig. 1A). Morphometric results at 7 days after NMDA injection of three to 10 independent experiments are shown in Fig. 2. As indicated by the morphologic analysis, the IPL in the NMDA-injected eye was thinner than in the contralateral saline-injected eye at 7 days after injection. No significant change was seen in the thickness of OPL and ONL after injection in all of the groups. Treatment with 15 mg/kg (the first two days) and 10 mg/kg (the following five days) (Fig. 1D), but not 5 mg/kg (the first two days) and 3 mg/kg (the following five days) (Fig. 1C), ATRA 60 min before NMDA injection significantly reduced the amount of retinal damage.

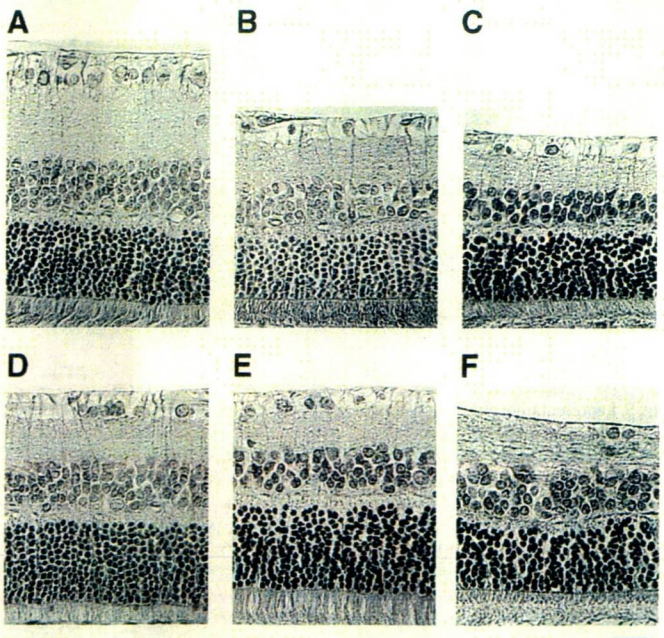

Fig. 1. Representative photomicrographs showing histological appearance of the vehicle-injected control (A), and NMDA-injected retinae 7 days after NMDA injection (B, C and D). ATRA was orally treated 60 min before NMDA injection. Retinal damage is shown in CMC (the vehicle of ATRA)-treated ($n=10$) (B), 5 mg/kg (the first two days) and 3 mg/kg (the following five days) ATRA-treated ($n=3$) (C) retinae. In the 15 mg/kg (the first two days) and 10 mg/kg (the following five days) ATRA-treated group, retinal structure is preserved ($n=8$) (D). The results of 45 mg/kg (the first two days) and 30 mg/kg (the following five days) ATRA-treated group could be divided into the two groups ($n=4$). Similar protective effects to those in the 15 mg/kg (the first two days) and 10 mg/kg (the following five days) ATRA-treated group was seen in 2 out of 4 animals (E), whereas no protection could be seen in others (F). Scale bar = 50 μm. Original magnification is ×200.

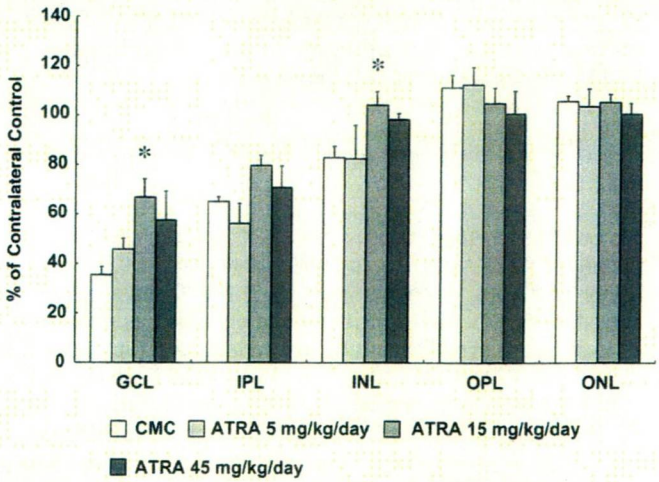

Fig. 2. Effect of ATRA treated orally on the histological damage induced by intravitreously NMDA injection. Retinal damage was examined 7 days after NMDA injection. The following 4 parameters of the NMDA-injected eyes were normalized to those of the vehicle-injected eyes (the opposite side of the NMDA-injected eye) and are presented as percentages: cell density in the GCL (ganglion cell layer) and the INL (inner nuclear layer); thickness of the IPL (inner plexiform layer), OPL (outer plexiform layer) and the ONL (outer nuclear layer). The data represent the means ± S.E.M. of three to ten rats per group. *$P<0.05$, vs. CMC-treated group.

The results of 45 mg/kg (the first two days) and 30 mg/kg (the following five days) ATRA-treated group could be divided into two groups. Similar protective effects to those in the 15 mg/kg (the first two days) and 10 mg/kg (the following five days) ATRA-treated group were seen in 2 out of 4 animals (Fig. 1E), whereas no protection could be seen in others (Fig. 1F). These results indicated that 15 mg/kg (the first two days) and 10 mg/kg (the following five days) ATRA is the best dose to protect against the NMDA-induced retinal damage. Oral treatment with ATRA itself did not affect the retinal morphology.

3.2. Effect of ATRA on apoptosis induced by the intravitreous NMDA injection in the rat retina

To examine whether ATRA reduces apoptotic cell death induced by intravitreous NMDA injection, we conducted TUNEL staining of the retina 6 h after NMDA injection. As shown in Fig. 3, TUNEL-positive cells were observed in the GCL and in the inner side of the INL, but not in the ONL, in the vehicle-treated group. Oral treatment with ATRA at

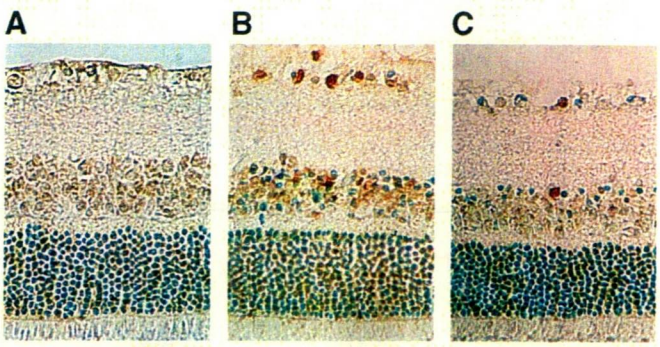

Fig. 3. Representative photomicrographs showing TUNEL staining of the vehicle-injected control and NMDA-injected retinae 6 h after NMDA injection. TUNEL-positive nuclei are shown in ganglion cell layer and inner nuclear layer of CMC (the vehicle of ATRA)-treated and NMDA-injected retinae ($n=4$) (B), whereas no TUNEL-positive cell was seen in CMC-treated and the vehicle of NMDA-injected retinae (the opposite side of the NMDA-injected eye) (A). In the retina treated with 15 mg/kg ATRA 60 min before NMDA injection, the number of the positive nuclei in the ganglion cell layer and the inner nuclear layer is smaller than that in the CMC and NMDA-treated retinae ($n=4$) (C). Scale bar = 50 μm. Original magnification is ×200.